Small ADP-ribosylation factor-like GTPase TITAN5 (TTN5/ARL2) is linked with the dynamic regulation of IRON-REGULATED TRANSPORTER1

Inga Mohr[1], Monique Eutebach[1], Naima Schommen[1], Regina Gratz[1], Kalina Angrand[2], Lara Genders[1], Tzvetina Brumbarova[1], Petra Bauer[1,3] and Rumen Ivanov[1]

[1]Institute of Botany, Heinrich Heine University, Universitätsstr. 1, 40225 Düsseldorf, Germany.
[2]former address: Department of Biosciences-Plant Biology, Saarland University, 66123 Saarbrücken, Germany.
[3]Cluster of Excellence on Plant Sciences (CEPLAS), Heinrich-Heine University, 40225 Düsseldorf, Germany.

Author contributions: P.B. and R.I. conceived the project; I.M., T.B., P.B. and R.I. designed experiments, supervised the research and analyzed data; I.M., M.E., N.S., R.G., and K.A. performed experiments; L.G. contributed key materials; I.M. wrote the manuscript; I.M., P.B. and R.I. edited the manuscript; P.B. acquired funding. P.B. and R.I. agreed to serve as the author responsible for contact and communication.

Highlights

- The small GTPase TITAN 5 (TTN5/ARL2) is linked to iron homeostasis
- TTN5 interacts with the large intracellular loop and variable region of IRON-REGULATED TRANSPORTER 1 (IRT1) and has a positive effect on root iron (Fe) reduction
- TTN5 interacts with peripheral membrane proteins of the IRT1 interactome, EHB1, PATL2 and SNX1 suggesting a coordinating role in IRT1 regulation
- TTN5 and IRT1 colocalize at the plasma membrane and the endomembrane system related to vesicle transport

Running title

ARF-like GTPase TTN5 and iron acquisition

One-sentence summary

ADP-ribosylation factor-like small GTPase TITAN 5 (TTN5/ARL2) links vesicle transport and iron homeostasis by binding the intracellular regulatory protein interaction region of IRON-REGULATED TRANSPORTER 1 (IRT1).

Keywords

ARF-like; ARLC1; ARL2; EHB1; endomembrane; GTPase; HALLIMASCH; iron; PATL2; plasma membrane; SEC14; SNX1; vesicle

Abstract

The endomembrane system is the central sorting machinery for membrane proteins where signals can be integrated to control plant nutritional responses. IRON-REGULATED TRANSPORTER1 (IRT1) is tightly controlled through trafficking between the endomembrane system and the plasma membrane to balance the demands for iron (Fe) and toxic effects that

may arise from excess of this micronutrient in roots. Small GTPases of the Ras superfamily regulate signaling inputs in endomembrane trafficking, but their functions and activities are poorly known in plants. One plant endomembrane system-associated regulatory component is the small ARF-like GTPase TITAN 5/ARL2/ARLC1/HALLIMASCH (hereafter termed TTN5). TTN5 is required during early embryo development but many open questions remain with regard to its physiological function during the later life cycle or in response to environmental cues. Here, we demonstrate that TTN5 interacts with IRT1vr, the large cytoplasmic variable region and protein-regulatory platform of IRT1. TTN5 also interacts with peripheral membrane proteins that are components of the IRT1 regulation machinery and can be involved in protein trafficking, like SNX1, the C2 domain protein EHB1 and the SEC14-GOLD domain-containing PATL2. We show that heterozygous *ttn5-1*$^{+/-}$ plants have a Fe reduction phenotype. Fluorescent fusion proteins of TTN5 and IRT1 colocalize at the plasma membrane and in endosomes/multivesicular bodies, where IRT1 sorting and cycling between the plasma membrane and the vacuole are coordinated. Hence, this work links IRT1 and iron nutritional regulation with a small GTPase. This opens up the possibility that iron nutrient levels are controlled *via* the cellular regulation of the endomembrane system.

Abbreviations

AD	activation domain
Arabidopsis	*Arabidopsis thaliana*
ARF-like / ARL	ADP-ribosylation factor-like
BD	binding domain
EE	early endosomes
EHB1	ENHANCED BENDING 1
FRET-APB	Förster Resonance Energy Transfer-Acceptor Photobleaching
GAP	GTPase-activating protein
GEF	guanine nucleotide exchange factor
ICQ	intensity correlation quotient
MVB	multivesicular body
PATL2	PATELLIN 2
ROI	region of interest
SNX1	SORTING NEXIN 1
TGN	*trans*-Golgi network
TTN5	TITAN 5
Y2H	yeast two-hybrid
ZIP	ZRT/IRT-LIKE PROTEIN

Introduction

Plants adjust to environmental changes, such as variations of soil nutrient availability. Cellular membranes are very dynamic in plants, and this is crucial for sessile organisms. Plants can scan their environment for nutrients and control the activities of plasma membrane transporter proteins by vesicular trafficking. Many open questions still exist with regard to the environmental responsiveness and the complexity of the plant cell endomembrane system.

One essential element, iron (Fe), is abundant in the soil. But since Fe is mostly present in insoluble ferric Fe complexes, it must be mobilized into a bioavailable form. Plants like

73 *Arabidopsis thaliana* (Arabidopsis) are capable of mobilizing ferric Fe^{3+} by reducing it *via*
74 plasma membrane FERRIC REDUCTION OXIDASE 2 (FRO2) (Robinson et al., 1999). The
75 reactive ferrous Fe^{2+} is taken up by IRON-REGULATED TRANSPORTER 1 (IRT1) into root
76 epidermis cells (Eide et al., 1996; Vert et al., 2002).
77 IRT1 is one of the founding members of the evolutionarily conserved ZIP (ZRT, IRT-LIKE
78 PROTEIN) divalent metal ion transporter family (Eide et al., 1996; Guerinot, 2000). Divalent
79 metal ions are potentially cytotoxic. The activity of IRT1, like that of other ZIP proteins, is
80 controlled at the level of protein abundance at the plasma membrane (Hu, 2021). In this
81 respect, IRT1 serves as a model system for studying the control of a ZIP transporter.
82 Importantly, IRT1 protein activity is controlled through transport from the *trans*-Golgi
83 network/early endosomes (TGN/EE) to the plasma membrane, degradation by the lytic
84 pathway and recycling back to the plasma membrane (Barberon et al., 2011; Shin et al., 2013;
85 Barberon et al., 2014; Foot et al., 2017; Zhang et al., 2023) and (Ivanov et al. 2014). The large
86 variable cytosolic region between transmembrane domains three and four (vr) is a
87 characteristic regulatory feature of ZIP proteins (Guerinot, 2000; Gaither and Eide, 2001). In
88 IRT1, this regulatory variable region, IRT1vr, is crucial for IRT1 control and target of metal ion
89 binding and post-translational modification (Grossoehme et al., 2006; Kerkeb et al., 2008;
90 Dubeaux et al., 2018; Cointry and Vert, 2019). Clearly, Fe acquisition is affected by regulation
91 of the vesicular transport mechanism, but how this is achieved and which proteins are involved
92 are open questions that still remain largely elusive.
93 Cycling of plasma membrane proteins is an important function of endomembrane trafficking
94 (Valencia et al., 2016; Ivanov and Vert, 2021). One protein family involved in this process in
95 mammalian cells and yeast is the Ras superfamily of small GTPases. Small GTPases are
96 important in vesicle-related processes as they function as molecular switches due to their
97 GTPase activities to transmit signals. Small GTPases have usually low intrinsic nucleotide
98 exchange and hydrolysis activity, and therefore, require the support of guanine nucleotide
99 exchange factors (GEFs) and GTPase-activating proteins (GAPs). GEFs recruit the inactive,
100 GDP-bound, GTPase to their site of action and lead to nucleotide exchange by GDP release.
101 GTP binding leads to a conformational change of two regions referred to as switch I and II. The
102 active, GTP-loaded, GTPases then exert their function, e.g. the recruiting and subsequent
103 assembly of coat proteins by ARF1 or SAR1, until hydrolysis of the GTP by GAPs. Most of the
104 known interactions occur in the active conformation of the GTPases (Sztul et al., 2019; Nielsen,
105 2020; Adarska et al., 2021). Although the ARF-GTPase family is well studied in mammals, there
106 are only few well-established examples of an ARF-GTPase functioning in plasma membrane
107 protein trafficking in plants, like that of ARF1-GNOM-mediated recycling of auxin carrier PIN
108 FORMED 1 (PIN1), with GNOM being an ARF-GEF (Steinmann et al., 1999; Geldner et al.,
109 2003). The presence of 21 ARF and ARF-like (ARL) GTPases encoded by the Arabidopsis
110 genome raises the question whether other ARF members may act in endomembrane trafficking
111 and what are their functions in the diverse physiological and nutrient assimilation pathways
112 besides auxin signaling and cell division.
113 TITAN5 (TTN5), also known as HALLIMASCH (HAL)/ARL2/ARLC1, is an ARF-like protein.
114 It was identified in two independent screens for abnormal-embryo mutants arrested soon after
115 egg cell division, indicating a central cellular function (Mayer et al., 1999; McElver et al., 2000),
116 in agreement with its ubiquitous expression in plants (Mohr et al., 2023). Physiological functions
117 of this small GTPase, relevant during other phases of the plant life cycle, remain elusive until
118 today. TTN5 is more closely related in sequence to human ADP-ribosylation factor-like2

119 (HsARL2) than any Arabidopsis protein. HsARL2 is associated with very diverse roles in cells,
120 ranging from microtubule development, also identified for yeast and Caenorhabditis homologs
121 (Bhamidipati et al., 2000; Fleming et al., 2000; Radcliffe et al., 2000; Antoshechkin and Han,
122 2002; Tzafrir et al., 2002; Mori and Toda, 2013), adenine nucleotide transport in mitochondria
123 (Sharer et al., 2002) and control of phosphodiesterase activity in cilia (Ismail et al., 2011; Fansa
124 and Wittinghofer, 2016). TTN5 orthologs are therefore not only involved in a diverse set of
125 functions and signaling cascades but they also bind very different protein partners for that.
126 *TTN5* is expressed in the root epidermis (Mohr et al., 2023), like *IRT1* (Vert et al., 2002). TTN5
127 is present at the plasma membrane and in the endomembrane compartment. Its unusually high
128 intrinsic GDP-GTP exchange activity, that causes TTN5 to be present predominantly in a GTP-
129 binding form, seems a prerequisite for its dynamic cellular localization (Mohr et al., 2023). TTN5
130 can be considered atypical as it does not require a GEF to be in its active GTP-bound form and
131 has a slow GTPase activity relying on a GAP (Mohr et al., 2023).
132 A yeast two-hybrid screen identified novel IRT1vr regulators (Khan et al., 2019; Hornbergs
133 et al., 2022). We report here, that with this same strategy, we retrieved the HsARL2 homolog
134 and small putative GTPase TTN5. We validated protein interactions of TTN5 and IRT1vr as
135 well as the IRT1vr interactome and found a physiological Fe reductase phenotype linked with
136 root Fe acquisition. Colocalization analysis indicated that the active GTP-bound TTN5 form
137 promoted the presence of IRT1 in intracellular vesicles. Hence, the dynamic small GTPase
138 TTN5 acts in a nutritional-environmental context in the vesicular trafficking system that serves
139 to control the presence of a root iron transporter at the plasma membrane.

140 Results

141 TTN5 interacts with the variable region of IRT1

142 To identify new cytoplasmic proteins regulating IRT1 we had developed a strategy for
143 identifying IRT1vr candidate interaction partners of IRT1vr (residues 145-192), and used
144 IRT1vr as bait against a cDNA expression library prepared from Fe-deficient Arabidopsis roots
145 (Khan et al., 2019). We report here that 25 of the colonies (representing 25 %) obtained in the
146 yeast two-hybrid (Y2H) screen carried a fragment of the coding sequence of the gene
147 AT2G18390, encoding the ARL-type small GTPase TTN5. We verified the interaction in a
148 targeted Y2H test (Figure 1A). Small GTPases act as molecular switches in cells, like it is the
149 case for TTN5 (Figure 1B) (Mohr et al., 2023). We further verified the protein interaction in plant
150 cells using Bimolecular Fluorescence Complementation (BiFC) as a reconstitution of YFP in
151 positively transformed cells that expressed the control marker mRFP (Figure 1C). We
152 generated mutants of conserved amino acids in the GTP-binding pocket, Thr30-to-Asn (T30N,
153 previously found to be dominant-negative and GDP-bound) and Gln70-to-Leu (Q70L,
154 characterized as dominant-active and GTP-bound) (Figure 1B) (Mohr et al., 2023). Both, the
155 dominant-negative cYFP-TTN5^{T30N} and active cYFP-TTN5^{Q70L} forms interacted with IRT1vr
156 (Figure 1D-E). The BiFC interactions were specific as neither protein partner was able to bind
157 negative controls in this assay (Figure 1F-G). We further elucidated whether IRT1vr might
158 discriminate between active and inactive TTN5 variant forms using a quantitative analysis of
159 the interaction by Förster Resonance Energy Transfer-Acceptor Photobleaching (FRET-APB).
160 This approach is based on close-proximity-dependent energy transfer of an excited GFP-
161 tagged TTN5 donor to a mCherry acceptor, here IRT1vr-mCherry. Energy transfer was
162 quantified as FRET efficiency (Figure 1H-J). FRET efficiencies between all GFP-TTN5 forms
163 and IRT1vr-mCherry were significantly higher compared to the donor-only sample, confirming

164 protein interactions between all TTN5 forms and IRT1vr. On the other hand, it still remains to
165 be shown that full-length IRT1 can interact with TTN5 at the membrane, e.g. by *in planta* pull-
166 down experiments of respective tagged proteins, an assay that was previously successful to
167 find hints for full-length IRT1-protein interactions with other peripheral membrane proteins
168 (Khan et al., 2019; Hornbergs et al., 2022).
169 In sum, we can conclude that TTN5 is a novel interactor of the cytoplasmic loop IRT1vr.
170 TTN5 is a link in the coordination of IRT1 regulation with vesicle trafficking. Surprisingly, the
171 GTP/GDP-binding conformations did not influence significantly the protein interaction in the
172 case of TTN5 with IRT1vr.
173

174 **TTN5 affects Fe homeostasis**

175 Following up on the IRT1-TTN5 interaction, we assumed that TTN5 might affect the
176 regulation of the Fe deficiency response. Homozygous TTN5 knock-outs are embryo-lethal
177 (Mayer et al., 1999; McElver et al., 2000), and heterozygous plants (*ttn5-1*$^{+/-}$) showed no
178 obvious developmental defects in comparison with wild type sibling plants (Figure 2A). Root
179 length increased under Fe deficient conditions but did not differ between wild type and *ttn5-1*$^{+/-}$
180 siblings, and chlorophyll content was not affected (Figure 2B-C). *TTN5* expression was nearly
181 50 % reduced in *ttn5-1*$^{+/-}$ compared to wild type siblings, consistent with single allele presence.
182 Very interestingly, we detected a 15 % decrease of *TTN5* gene expression between Fe
183 sufficiency and deficiency in wild type and *ttn5-1*$^{+/-}$, indicating that TTN5 might be perhaps less
184 needed under low Fe supply (Figure 2D). We examined the heterozygous seedlings at the
185 molecular and physiological level. No difference of gene expression levels of *FRO2* and *IRT1*
186 occurred in *ttn5-1*$^{+/-}$ roots compared with wild type (Figure 2E-F). This indicated that root Fe
187 deficiency responses might not be compromised in *ttn5-1*$^{+/-}$. However, we then noted that in
188 two out of three experiments (each including the indicated biological replicates), Fe reductase
189 activity was altered. It was up-regulated under Fe-deficient versus -sufficient conditions in wild
190 type and *ttn5-1*$^{+/-}$ roots, but upon Fe deficiency, Fe reductase activity was reduced in *ttn5-1*$^{+/-}$
191 compared with wild type siblings (Figure 2G).
192 Taken together, heterozygous *ttn5-1*$^{+/-}$ seedlings have an Fe reductase phenotype that
193 indicates a positive effect of TTN5 at the physiological level of Fe acquisition. This was
194 interesting, because two other interactors of IRT1vr had an opposite effect on Fe reductase
195 activity. The C2 domain protein EHB1/CAR6 had a negative effect and also the SEC14 protein
196 PATELLIN 2 (PATL2) (Khan et al., 2019; Hornbergs et al., 2022).
197

198 **TTN5 colocalizes with IRT1 in endocytosed plasma membrane material**

199 To investigate how TTN5 may interact with IRT1, we compared localization of IRT1-mCitrine
200 (proIRT1::IRT1-mCitrine/*irt1-1*) (Dubeaux et al., 2018) with YFP-TTN5 (pro35S::YFP-TTN5) in
201 the root. The YFP-TTN5 fusion protein was found to be localized at the plasma membrane and
202 in the endomembrane system, where IRT1 is present, in a similar manner as
203 immunolocalization signals of a complementing HA_3-TTN5 protein (Mohr et al., 2023). 6-day
204 old transgenic Arabidopsis plants of the TTN5 and IRT1 reporter fusion lines were grown side-
205 by-side (Supplemental Figure S1). As previously described, IRT1-mCitrine was present at the
206 plasma membrane of root epidermis cells in our growth system (Supplemental Figure S1A)
207 (Dubeaux et al., 2018; Hornbergs et al., 2022). The same was the case for YFP-TTN5
208 (Supplemental Figure S1B), corresponding to the previously identified pattern (Mohr et al.,

209 2023). Virtual cross sections of both constructs highlighted the polar expression of IRT1-
210 mCitrine (Supplemental Figure S1C) compared with an equally distributed YFP-TTN5 in the
211 epidermis (Supplemental Figure S1D). Next to plasma membrane localization both, IRT1-
212 mCitrine and YFP-TTN5 were expressed in vesicle-like structures in root cells (Supplemental
213 Figure S1E-F). These findings suggested that IRT1 and TTN5 may locate to similar structures
214 inside root cells, supporting an interaction at these places.
215 To confirm the obtained Arabidopsis data and to investigate potential colocalization of TTN5
216 with IRT1, we used the transient expression system of *Nicotiana benthamiana*. We created a
217 constitutively expressing GFP-tagged IRT1 with GFP inserted inside the cytoplasmic loop
218 (hereafter termed IRT1-GFP). This IRT1 fusion protein was present at the plasma membrane.
219 Fluorescent spots were also found in close proximity to the plasma membrane (Supplemental
220 Figure S2A), consistent with previous reports (Barberon et al., 2011; Ivanov et al., 2014). To
221 further evaluate its usefulness for localization studies, we compared IRT1-GFP signals with
222 already described C-terminally-tagged IRT1-mCherry signals in transformed *N. benthamiana*
223 cells (Ivanov et al., 2014) before and after wortmannin treatment. Wortmannin is a fungal
224 metabolite with an inhibitory effect on phosphatidylinositol-3-kinase (PI3K) function, leading to
225 swollen multivesicular bodies (MVBs) and therefore is commonly used to investigate
226 endocytosis (Cui et al., 2016). The two constructs showed good colocalization and, following
227 wortmannin treatment, could be observed among others in swollen structures, suggesting
228 partial presence in the MVBs (Supplemental Figure S2B-C), indicating that the new IRT1-GFP
229 construct was suited for IRT1 localization studies. IRT1-GFP complemented an early rosette
230 growth deficit of *irt1-1* (in pro35S::IRT1-GFP/*irt1-1* plants), indicating functionality of the IRT1-
231 GFP construct for this trait (Supplemental Figure S2D).
232 We detected colocalization of IRT1-GFP and the three different mCherry-TTN5 constructs at
233 the plasma membrane (Figure 3A-C). We found YFP-TTN5 localization in vesicle-like
234 structures and close proximity of YFP-TTN5 to the plasma membrane, as previously reported
235 (Mohr et al., 2023). YFP-TTN5^{T30N} is less mobile than TTN5 and TTN5^{Q70L} (Mohr et al., 2023).
236 Further investigation revealed a significant colocalization difference between the inactive and
237 active variant of TTN5 with IRT1 (Supplemental Figure S2E). While Pearson coefficients of
238 IRT1-GFP with mCherry-TTN5 and mCherry-TTN5^{Q70L} were 0.77 and 0.80 respectively, it was
239 0.90 for IRT1-GFP and mCherry-TTN5^{T30N}, demonstrating higher general colocalization
240 between IRT1-GFP and the low-mobile low-activity TTN5 form (Supplemental Figure S2E;
241 similar results for overlap coefficients). All three mCherry-TTN5 constructs were also localized
242 in IRT1-GFP-positive structures close to the plasma membrane, suggesting the two proteins
243 might colocalize in plasma membrane-derived vesicles (Figure 3D-F). Surprisingly, the
244 Pearson coefficients changed when these spotted structures were analyzed (Supplemental
245 Figure S2F; similar results for overlap coefficients). While the values for mCherry-TTN5 (0.80)
246 and mCherry-TTN5^{Q70L} (0.78) with IRT1-GFP remain relatively the same, we obtained with 0.78
247 now a similar coefficient with mCherry-TTN5^{T30N}. Similar results were achieved while checking
248 the overlaps of mCherry-TTN5 structures with IRT1-GFP, with overlaps of 36-41 %
249 (Supplemental Figure S2G). In contrast, only 54 % of IRT1-GFP-positive structures colocalized
250 with mCherry-TTN5^{T30N}, whereas 61 % and up to 83 % colocalized with mCherry-TTN5 and
251 mCherry-TTN5^{Q70L}, respectively. From this, we hypothesized that IRT1 along with dominant
252 negative TTN5 is more likely to be localized at the plasma membrane while the active variant
253 may play a role in intracellular cycling. This was consistent with the previous observation that
254 YFP- TTN5^{T30N} was moving slower in the cell than the other two TTN5 fusion proteins, indicating

255 that it might have led to a slow-down of IRT1 removal from the plasma membrane. In an attempt
256 to identify the intracellular structures, we treated the cells with wortmannin (Figure 3G).
257 Structures positive for both IRT1-GFP and mCherry-TTN5 became doughnut-shaped
258 suggesting IRT1-TTN5 colocalization in MVBs (Figure 3H-J). Presence of IRT1 in these late
259 endosomal compartments has been observed previously, as part of the pathway to IRT1
260 vacuolar degradation (Dubeaux et al., 2018), same for YFP-TTN5 (Mohr et al., 2023). Thus,
261 our findings emphasize the involvement of TTN5 in the endomembrane trafficking of the Fe
262 transporter IRT1.
263

264 **TTN5 interacts with IRT1 regulators EHB1, SNX1 and PATL2**

265 We previously found that IRT1 associates and colocalizes with certain peripheral membrane
266 proteins. To further undermine that TTN5 associates with IRT1, we investigated the possibility
267 that TTN5 also binds these other proteins of the IRT1 interactome in close proximity.
268 At first, we tested IRT1-interacting C2-domain protein ENHANCED BENDING 1 (EHB1)
269 (Khan et al., 2019) that belongs to the ten-member calcium-dependent C2-DOMAIN ABSCISIC
270 ACID-RELATED (CAR) protein family (EHB1 is also known as CAR6) (Rodriguez et al., 2014).
271 CAR proteins tether signaling and transport proteins involved in drought, defense or iron
272 nutrition to the membrane (Cui et al., 2023). They can also oligomerize and cause membrane
273 deformations, making them candidate proteins involved in vesicle budding (Chen et al., 2023).
274 CAR proteins have a plant-specific insertion of an extra region within the C2 domain known as
275 signature (sig) domain, that is involved in binding proteins (Rodriguez et al., 2014; Khan et al.,
276 2019). EHB1 interacts *via* its sig domain with IRT1vr and it has an inhibitory effect on Fe
277 acquisition (Khan et al., 2019). Interestingly, while EHB1Δsig did not interact with TTN5 in BiFC,
278 the intact EHB1 protein and the EHB1 sig domain alone interacted with TTN5 in BiFC (Figure
279 4A-C, see also Figure 1F). FRET-APB experiments were used for validation taking EHB1-GFP
280 as the donor sample and all three TTN5 variants as the acceptor with a C-terminal mCherry-
281 tag. EHB1-GFP with TTN5-mCherry yielded a significantly higher FRET efficiency compared
282 to the donor-only sample (Figure 4F). Surprisingly, the FRET pairs EHB1-GFP with $TTN5^{T30N}$-
283 mCherry and $TTN5^{Q70L}$-mCherry resulted in an even higher FRET-efficiency compared to TTN5
284 (Figure 4F).
285 SORTING NEXIN 1 (SNX1) is a positive regulator of IRT1 recycling at the TGN (Ivanov et
286 al., 2014). TTN5 was able to bind SNX1 (Figure 4G). The active TTN5 GTPase variant
287 interacted with SNX1 (Figure 4I), while the inactive TTN5 mutant failed (Figure 4H). Sorting
288 nexins are classified by their characteristic domains. SNX1 represents the class I SNX proteins,
289 characterized by the presence of PHOX-homology (PX) and Bin-Amphiphysin-Rvs (BAR)
290 domains (Heucken and Ivanov, 2018). Such a domain organization is typical for proteins that
291 function in membrane and phosphoinositide binding by the PX domain, whereas the BAR
292 domain is involved in membrane curvature sensing and the formation of endosomal tubules
293 (Peter et al., 2004; Frost et al., 2009). Interestingly, ARF-GAPs which are needed for the GTP
294 hydrolysis, contain a BAR domain as well (Memon, 2004). We found evidence that TTN5 binds
295 to both the SNX1 PX and BAR domains using BiFC (Figure 4J-K).
296 Lastly, plasma membrane-localized SEC14 protein PATELLIN 2 (PATL2) binds IRT1vr
297 (Hornbergs et al., 2022). The SEC14 domain is a lipid-binding pocket that serves to present or
298 transfer lipophilic substances at membranes (Montag et al., 2023). Thereby, PATL2 is a lipid
299 transfer protein that may connect oxidative stress prevention and Fe acquisition, possibly by

transferring and exchanging phospholipids and α-tocopherol at the membrane. PATL2 may also initiate vesicle formation (Hornbergs et al., 2022). We tested interaction ability of cYFP-TTN5 with nYFP-PATL2 in BiFC experiments. YFP signals indicating complementation and interaction were visible at the plasma membrane, fitting to the localization studies of both PATL2 and TTN5 (Figure 4L). We were not able to observe complementation for the combination of PATL2 and any of the two GTPase variants $TTN5^{T30N}$ (Figure 4M) and $TTN5^{Q70L}$ (Figure 4N). This was very interesting, as it indicates that the TTN5 switching mechanism may be required for a potential interaction between these two proteins. To further identify the region of interaction, we tested already published deletion mutants of PATL2 (Montag et al., 2020). PATL2 can be divided into two protein halves, consisting of the N-terminal part and the conserved C-terminal CRAL-TRIO-N-terminal extension (CTN), SEC14 and Golgi dynamics (GOLD) domains of PATL2 (Montag et al., 2020). The N-terminal part is needed for the interaction with IRT1vr (Montag et al., 2020). We used the PATL2 deletion mutants nYFP-PATL2ΔC lacking the three consecutive CTN, SEC14-GOLD domain and nYFP-PATL2ΔN lacking the IRT1vr-interacting N-terminal part. nYFP-PATL2ΔC together with cYFP-TTN5 complemented YFP (Figure 4O), whereas no signal was obtained by nYFP-PATL2ΔN in combination with cYFP-TTN5 (Figure 4P), similar as in the case of IRT1vr (Hornbergs et al., 2022). Interestingly, the fluorescent complementation signal between cYFP-TTN5 and nYFP-PATL2ΔC was no longer present at the plasma membrane consistent with the observation that the PATL2 plasma membrane localization is dependent on C-terminal PATL2 domain region (Montag et al., 2020).

We also analyzed *EHB1, SNX1* and *PATL2* gene expression. All genes were expressed in similar levels in both wild type and *ttn5-1*$^{+/-}$ (Supplemental Figure S3A-C) indicating that there was no feedback at the level of regulation of genes encoding the TTN5 interactors.

In summary, we could show that TTN5 is not only interacting with IRT1vr but also with three peripheral membrane proteins that can be in the vicinity of IRT1 at membrane sites in root cells. This suggests formation of a protein complex at the IRT1vr regulatory platform in which TTN5 may have a coordinating role due to its switch mechanism.

Discussion

Here, we show that the small GTPase TTN5 links Fe homeostasis with the endomembrane trafficking system (Figure 5). We demonstrate that TTN5 interacted with the large intracellular loop and variable region of IRT1 and colocalized with IRT1 in plant cells at the plasma membrane and in vesicle structures. TTN5 had a positive effect on root iron reduction. *TTN5* gene expression was found to be slightly lower upon Fe deficiency than sufficiency. TTN5 interacted with peripheral membrane proteins of the IRT1 interactome, EHB1, PATL2 and SNX1. Hence, our findings shed new light on a post-embryonic physiological ARL GTPase function in plant nutrition. Binding of TTN5 directly to the cargo IRT1 *via* IRT1vr indicates specificity of TTN5 function beyond housekeeping roles. The concert with Ca^{2+}-dependent and oxidative stress-related proteins, EHB1 and PATL2, as well as protein sorting by SNX1 indicate that TTN5 links dynamic plasma membrane and vesicle trafficking responses with Fe regulation to control an iron transporter. Nucleotide exchange and GTPase activities of TTN5 were important for several of the mentioned activities since respective mutants of TTN5 showed partly different behavior from TTN5.

345 **TTN5 is part of the endomembrane system, targeting IRT1vr**

346 The interaction between TTN5 and IRT1vr is supported by multiple findings. First, the
347 interaction was detected in a Y2H screen, that yielded only few interaction partners, which
348 could all be validated. Second, the interaction was verified by using independent methods
349 (targeted Y2H, BiFC and FRET-APB). Third, TTN5 and IRT1 reporter proteins colocalized in
350 cells, and their localization overlapped in intracellular membrane-associated locations in cells
351 of the root epidermis, in which both genes and proteins are expressed and present according
352 to transcriptome studies and promoter reporter lines. Further, TTN5 was found to interact with
353 proteins of the IRT1vr environment (Figure 5A-B). These findings altogether indicate that in
354 plant roots, TTN5 and IRT1 indeed can be present to interact in root epidermis cells in places
355 related with Fe acquisition. Since TTN5 is involved in vesicle trafficking, like other members of
356 the ARF family of small GTPases (Memon, 2004; Sztul et al., 2019) it has diverse localization
357 patterns within the cell. The previous TTN5 localization (Mohr et al., 2023) was confirmed upon
358 colocalization with IRT1 in this study. Hence, IRT1 localization dependent on endomembrane
359 trafficking may be linked with the presence of TTN5 in this process.

360 A very interesting finding was that the dominant-negative mCherry-TTN5^{T30N} variant tended
361 to colocalize more at the plasma membrane with IRT1-GFP while intracellular vesicle-like
362 structures of IRT1-GFP overlapped more with the active mCherry-TTN5 variant. This is
363 consistent with our colocalization data with the Golgi, MVB and plasma membrane markers
364 (Mohr et al., 2023) and reinforces our suggestion that TTN5 has functions in vesicle trafficking.
365 Since TTN5^{T30N} is predicted to strongly bind a GEF, we can suppose that TTN5^{T30N} presence
366 at the plasma membrane might be linked with a TTN5-interacting GEF at this site. The presence
367 of mCherry-TTN5 together with IRT1-GFP in wortmannin-induced swollen structures, probably
368 indicating MVBs, is supporting the idea of a role in transporter degradation. MVBs are known
369 to be the last step before vacuolar degradation (Kolb et al., 2015; Arora and Van Damme,
370 2021). This could indicate that TTN5 presence is a critical point of IRT1 sorting fate. We
371 therefore propose a role of TTN5 in targeting intracellular IRT1 protein (Figure 5B). In this
372 process, TTN5 is present at the plasma membrane in a resting state. In the move of GTPase
373 activation, it could be recruited to the place of action and active TTN5 would play a role in IRT1
374 cycling. TTN5 should predominantly bind GTP and be in an active state in the cell (Mohr et al.,
375 2023). Further, there is support of a role of TTN5 in IRT1 recycling by the binding of TTN5 and
376 SNX1. SNX1 is involved in the recycling of IRT1 at these sites (Ivanov et al. 2014). Hence,
377 TTN5 can be in a functional complex with SNX1 to control the recycling of the cargo protein
378 IRT1.

379 The observed roles of TTN5 fit well with the general understanding of ARF-signaling in
380 plasma membrane protein trafficking. The auxin transporters PIN1 and PIN2 and the boron
381 transporter BOR1, like IRT1, are polar localized in the plasma membrane and undergo a
382 constant degradation-recycling process (Benková et al., 2003; Takano et al., 2010; Barberon
383 et al., 2014). Apart from vesicle formation, as described for ARF1 or SAR1, a role in this process
384 was shown for other regulatory mechanisms of ARF-signaling through the GEFs and GAPs
385 (Nielsen, 2020). GNOM and BIG5, two ARF-GEFs, and ARF1-regulators, are described to be
386 involved in the proper localization of the plasma membrane transporter PIN1, functioning at
387 different regulatory steps (Geldner et al., 2003; Anders et al., 2008; Kleine-Vehn et al., 2008;
388 Tanaka et al., 2009). In addition, another ARF GTPase ARF1A1C may not only partially
389 colocalize with GNOM, but modified activity also resulted in impaired localization of PIN1 to the
390 plasma membrane and also altered vacuolar targeting of PIN2 (Tanaka et al., 2014). BOR1

391 plasma membrane localization depends on GNOM as well (Yoshinari et al., 2021), showing a
392 good connection between ARF-GEFs and plasma membrane protein localization.
393 A limitation in our study was that we were not able to show TTN5 interaction with full-length
394 IRT1 by coimmunoprecipitation. This might have been due to a transient interaction.
395 Alternatively, fluorescent protein-based interactions approaches are often limited by technical
396 issues, e.g. a spatial distance of the fluorescent proteins. Perhaps the locations of the tags can
397 be problematic for certain interactions like that of TTN5 and IRT1.
398 Taken together, we could not only identify TTN5 as part of the endomembrane system but
399 also uncover another link between ARF signaling and plasma membrane protein trafficking by
400 its interaction with IRT1vr. Future identification of potential TTN5-GEF and -GAP proteins will
401 be of great interest to clarify the role of TTN5 in endomembrane trafficking with particular
402 reference to IRT1 regulation. For future studies, stable coexpression of both proteins under the
403 control of the endogenous promoter will be suitable to investigate the effect of TTN5 on IRT1.
404

405 **TTN5 might play a general role in Fe nutrition**

406 TTN5 does not only have an influence on IRT1 but rather potentially possesses a general
407 role in Fe nutrition. A partial lack of TTN5 results in decreased Fe reductase activity. It was
408 already investigated that IRT1 can interact with FRO2 and AHA2 and potentially form a complex
409 for a highly effective Fe uptake machinery (Martín-Barranco et al., 2020). Reduced Fe
410 reductase activity could be due to an indirect influence of TTN5 on the complex formation or it
411 could be directly driven by TTN5. Interestingly, both *ehb1* and *patl2* seedlings have a higher
412 Fe reductase activity under Fe deficiency compared to wild type suggesting an opposing role
413 of TTN5 on the Fe deficiency response. Gene expression analysis revealed no great impact on
414 Fe-related genes in *ttn5-1*$^{+/-}$ roots, implying an effect of TTN5 mostly on posttranslational level.
415 It is a possibility that TTN5 has very different effects depending on its localization in the cell.
416 For example, the effect on Fe reduction could be different from its effect on colocalization with
417 IRT1 in MVBs. Different types of interaction partners were reported for the human homolog
418 ARL2 with connection to distinct cellular functions in tubulin folding and microtubule dynamics
419 (Bhamidipati et al., 2000) or in mitochondria (Sharer et al., 2002). Based on these distinct
420 locations and the associated functions of ARL2, it was proposed that ARL2 may act at a high
421 level in signaling (Francis et al., 2016). This can be also the case in Arabidopsis. For example,
422 TTN5 may bridge TTN5 microtubule function (Mayer et al., 1999) with our here-found role in
423 IRT1 regulation.

424

425 **TTN5 interacts with EHB1, SNX1 and PATL2 and may coordinate IRT1 regulation**

426 It is already known that IRT1 regulation is a process of high complexity which is not only
427 influenced by Fe-sufficient or -deficient conditions, but also by other metals such as zinc and
428 manganese or Ca^{2+}- and ROS-signaling among others (Dubeaux et al., 2018; Brumbarova and
429 Ivanov, 2019; Khan et al., 2019; Gratz et al., 2021).
430 Interaction with the IRT1 regulators EHB1, PATL2 and SNX1 suggests that TTN5 could not
431 only be linked with Fe nutrition but also the associated Ca^{2+}- and ROS-signaling events,
432 previously studied for EHB1 and PATL2 (Khan et al. 2019; Hornbergs et al. 2022). We identified
433 interaction with EHB1 by two independent methods (BiFC and FRET-APB) and with PATL2
434 and SNX1 by BiFC. The interactions are further supported by deletion mutant approaches. The
435 interacting sites of PATL2 and EHB1 with TTN5 were similar to those for IRT1vr, supporting

436 again the possibility that these domains and motifs are at the basis of a protein complex forming
437 at the IRT1vr regulatory platform.
438 Fe deficiency leads to an increase of cytosolic Ca^{2+} (Gratz et al., 2019; Matthus et al., 2019).
439 Physiological data indicate that CBL1/9-dependent CIPK23 activation is promoting an induction
440 of the Fe reductase activity (Tian et al., 2016). Contrary to this, CBL1/9 are also responsible
441 for potential IRT1 endocytosis by CIPK23-dependent phosphorylation and the transporter
442 activity is inhibited by Ca^{2+}-induced recruiting of EHB1 to the plasma membrane (Dubeaux et
443 al., 2018; Khan et al., 2019), suggesting opposing effects of Ca^{2+} in the Fe deficiency response.
444 EHB1 is additionally interesting as a member of the CAR family. Several CAR proteins can
445 initiate Ca^{2+}-dependent membrane curvature, which may provide a direct link to vesicle
446 trafficking. Interestingly, Ca^{2+} is bound by EHB1 *via* its C2 domain, which is also a common
447 feature of class III ARF-GAPs (Vernoud et al., 2003; Knauer et al., 2011). Indeed, EHB1 is
448 directly linked to ARF signaling in an antagonistic interaction with ARF-GAP AGD12 in
449 gravitropic bending (Dümmer et al., 2016; Rath et al., 2020). Further research needs to
450 investigate whether TTN5 can interact with the C2-domain containing ARF-GAPs AGD11-
451 AGD13 as well. Additionally, crystallization experiments revealed a potential Ca^{2+}-binding site
452 between HsARF6 and its GAP ASAP3. The GTP-hydrolysis was stimulated in the presence of
453 Ca^{2+} proposing a linkage between Ca^{2+}- and ARF-signaling (Ismail et al., 2010). We therefore
454 consider the possibility of an interaction between TTN5 and EHB1 in a Ca^{2+}-dependent manner.
455 PATL2 may interact with IRT1 to prevent lipid peroxidation stress (Hornbergs et al., 2022).
456 Prolonged Fe deficiency leads to an increase in hydrogen peroxide concentration as well as an
457 activity increase of catalase CAT2 (Le et al., 2015; von der Mark et al., 2020; Gratz et al., 2021).
458 Some catalases are present in the PATL2 interactome in roots (Hornbergs et al., 2022). Future
459 studies may address whether TTN5 is connected with oxidative stress.
460 Next to EHB1 and PATL2, we identified SNX1 as a positive regulator for IRT1 recycling to
461 the plasma membrane in the sorting endosomes (Ivanov et al., 2014). In addition to IRT1,
462 endosomal recycling of the auxin efflux carrier PIN2 is also dependent on SNX1 (Jaillais et al.,
463 2006). SNX1 is therefore part of the recycling of specific plasma membrane proteins.
464 Interestingly, deficiency of BLOS1 leads to accumulation of PIN1 and PIN2 at the plasma
465 membrane (Cui et al., 2010). BLOS1 is one of the homologs to the mammalian biogenesis of
466 lysosome-related organelles complex 1 (BLOC-1), which is responsible for vesicle transport
467 from endosomes to lysosomes (Li et al., 2007; Raposo et al., 2007). BLOS1 could therefore
468 perform a similar function to BLOC-1 in Arabidopsis. SNX1 can interact with both BLOS1 and
469 BLOS2 and could therefore also play a role in vesicle-mediated transport through these
470 interactions (Cui et al., 2010; Heucken and Ivanov, 2018). SNX1 possesses a BAR domain
471 which is also typical for class I ARF-GAPs (Vernoud et al., 2003; Heucken and Ivanov, 2018).
472 A connection between the SNX1 BAR domain and an ARF6-GEF was identified in mouse by
473 their interaction. This interaction was associated with a positive effect of ARF6 function (Fukaya
474 et al., 2014). Colocalization analysis revealed overlapping expression in endosomes, which fits
475 known SNX1 localization in Arabidopsis (Fukaya et al., 2014; Ivanov et al., 2014), this could be
476 a possible interconnection between ARF-signaling and SNX1. Here, we identified an interaction
477 between TTN5 and SNX1, which could be the critical link in the decision between SNX1-
478 dependent recycling and degradation of IRT1. SNX1 could be needed for a potential TTN5-
479 GEF and subsequent TTN5 recruiting to membranes. Based on the opposing roles of EHB1
480 and SNX1 in IRT1 regulation and their here-described connection to TTN5, we suggest a
481 coordinating role of TTN5 in transporting IRT1 between plasma membrane and endosomes by

482 interacting with its regulators such as EHB1, PATL2 and SNX1. The findings that some ARF-
483 GAPs have a C2 or BAR domain, and that SNX1 interacts with an ARF-GEF strengthen the
484 interest in the identification of TTN5-GEFs and -GAPs.
485 Further research has to focus on physiological aspects in either combined knockout mutants
486 or tagged-protein lines to arrange and decipher the IRT1 regulatory network. An intriguing open
487 question is whether a large IRT1vr-EHB1-PATL2-TTN5-SNX1 complex is assembled. If so, the
488 next question is how, when and in which order the individual or all components of the IRT1vr
489 complex are assembled. Another question is which are the structural requirements for proper
490 protein conformations and membrane interfaces (Figure 5A, B).

491 **Conclusion and perspectives**

492 In this study, we identified the ARF-like GTPase TTN5 as an interactor of the iron transporter
493 IRT1 and three of its known regulators, SNX1, PATL2 and EHB1, suggesting that they form a
494 complex at the IRT1vr site. One role of TTN5 and perhaps the entire identified IRT1vr complex
495 including TTN5 is likely to contribute to endocytosis and recycling of IRT1. The proposed model
496 of complex formation to affect IRT1 localization at the plasma membrane can be studied further
497 in the future. TTN5 manipulation can show whether indeed TTN5 affects IRT1 endocytosis and
498 degradation or its recycling. Furthermore, certain physiological effects may facilitate that a
499 complex forms composed of TTN5 with PATL2, EHB1 and SNX1, also in combination with
500 IRT1. An intriguing question is whether TTN5 binds specifically with IRT1 or also targets other
501 transmembrane cargo proteins. A challenging task is to obtain proofs of TTN5 protein
502 complexes of this kind in roots and determine the requirements and order of events for complex
503 assembly. Finally, due to the very low intrinsic GTP hydrolysis activity of TTN5, identification of
504 TTN5 GAPs will shed light on TTN5 function in Fe homeostasis and potential other cellular
505 signaling events. Likewise, it will be interesting to identify a membrane-localized GEF of TTN5.

506 **Material & Methods**

507 **Yeast two-hybrid (Y2H)**

508 The yeast two-hybrid screen for identification of IRT1vr interactors was performed previously
509 and is described in Khan et al. (2019). Targeted Y2H interactions were tested using the GAL4
510 transcription factor system with histidine as selection marker. *TTN5* coding sequence was
511 amplified using TITAN5 nter B1 and TITAN5 stop B2 primers (for primer sequences, see
512 Supplemental Table S1). Obtained fragment was cloned into pDONR207 *via* Gateway BP
513 reaction with following LR reactions into pGBKT7-GW (binding domain, BD) or pACT2-GW
514 (activation domain, AD). Both vectors were a kind gift from Dr. Yves Jacob. The yeast strain
515 AH109 was cotransformed with the corresponding AD- and BD-tagged expression vectors. The
516 combination pACT2:SNX1 and pGBKT7:SNX1 (Pourcher et al., 2010) was used as a positive
517 control. Negative controls were cotransformations with the respective non-recombined pACT2-
518 GW or pGBKT7-GW. Drop test was performed with SD -Leu, -Trp-cultures at an OD_{600} of 0.1
519 and three additional 1:10 dilution steps (10^1-10^4) on SD -Leu, -Trp- and SD -Leu, -Trp, -His +
520 0,5 mM 3-amino-1,2,4-triazole-plates. One of each plate was incubated either at 30°C or at
521 room temperature, wrapped in aluminum foil for up to two weeks.

522 **Arabidopsis plant material and growth conditions**

523 The Arabidopsis *ttn5-1* mutant was previously described (McElver et al., 2000).
524 Heterozygous seedlings were selected by PCR on gDNA using the primer TTN5 intron1 fwd
525 and pDAP101 LB1 (Supplemental Table S1). Arabidopsis seeds were sterilized with sodium

526 hypochlorite solution (6 % Sodium hypochlorite and 0.1 % Triton X-100) and stored 24 hours
527 at 4°C for stratification. Seedlings were grown upright on Hoagland media [1.5 mM $Ca(NO_3)_2$,
528 0.5 mM KH_2PO_4, 1.25 mM KNO_3, 0.75 mM $MgSO_4$, 1.5 µM $CuSO_4$, 50 µM H_3BO_3, 50 µM KCl,
529 10 µM $MnSO_4$, 0.075 µM $(NH_4)_6Mo_7O_{24}$, 2 µM $ZnSO_4$ and 1 % sucrose, pH 5.8, supplemented
530 with 1.4 % Plant agar (Duchefa)] with sufficient (50 µM FeNaEDTA, +Fe) or deficient (0 µM
531 FeNaEDTA, -Fe) Fe supply in growth chambers (CLF Plant Climatics) under long day condition
532 (16 hours light at 21°C, 8 hours darkness at 19°C). Seedlings were grown in a two-week growth
533 system with plants growing 14 days on Fe-sufficient media and then transferred to either fresh
534 Fe-sufficient or Fe-deficient media for additional three days.
535 *Nicotiana benthamiana* plants were grown on soil for 2-4 weeks in a greenhouse facility
536 under long day conditions (16 hours light, 8 hours darkness).

537 **Root length**

538 For root length comparison plants were growing for 10 days in Fe-sufficient or -deficient
539 conditions photographed including a scale in the picture. Root length were measured from root
540 tip to hypocotyl using the JMicro Vision program (Roduit, N. JMicroVision: Image analysis
541 toolbox for measuring and quantifying components of high-definition images. Version 1.3.4.
542 https://jmicrovision.github.io) (+Fe: WT n = 19; *ttn5-1* n = 28; -Fe: WT n = 16; *ttn5-1* n = 32).

543 **Chlorophyll content**

544 For chlorophyll content comparison plants were grown in the two-week system in Fe-
545 sufficient or -deficient conditions. Chlorophyll content was measured by SPAD values using
546 SPAD-502plus (Konica Minolta Optics, 2012) with up to ten biological replicates (+Fe: n = 10;
547 -Fe: n = 9). Chlorophyll content was determined in three individual experiments.

548 **Fe reductase activity assay**

549 Fe reductase activity assay was performed as described in (Gratz et al., 2019). For Fe
550 reductase activity plants were grown in the two-week system in Fe-sufficient or -deficient
551 conditions. Two plants per replicate were washed in 100 mM $Ca(NO_3)_2$, then incubated for
552 1 hour in the dark in 1.5 ml Fe reductase solution (300 mM ferrozine and 100 mM FeNaEDTA).
553 The Fe reductase activity-dependent color change was measured at 562 nm using Infinite
554 200® PRO (Tecan) plate reader. Activity calculation was done using the ferrozine extinction
555 coefficient $\varepsilon = 28.6\ mM^{-1}*cm^{-1}$ and was normalized to root weight. The assay was performed
556 with a minimum of three replicates ($n \geq 3$), each consisting of a pool of two plants. Fe reductase
557 activity was determined in three individual experiments.

558 **Rosette size**

559 For rosette size measurements plants were grown in parallel for one week in Fe-sufficient
560 conditions on Hoagland plates before transferring them to soil. 14 days after sowing rosette
561 sizes was measured using ImageJ (Schneider et al., 2012). The size was determined between
562 tips of opposite leaves of twelves plants each (n = 12).

563 **Gene expression analysis by RT-qPCR**

564 For gene expression analysis, plants were grown in the two-week system. Total RNA was
565 isolated from roots using the RNeasy Mini Kit (Qiagen) and cDNA synthesis was performed
566 with the RevertAid RT Reverse Transcription Kit (ThermoFisher Scientific). The SFX96
567 Touch™Real-Time PCR Detection System (Bio-Rad) was used for RT-qPCR performance.
568 Data processing was done with Bio-Rad SFX Manager™ (version3.1) software. Mass standard
569 curve analysis was used for determination of the absolute gene expression and the elongation

570 factor *EF1Bα* expression served as a reference for normalization. RT-qPCR was performed in
571 three biological replicates (n = 3) and two technical replicates each. All primer pairs used in this
572 study are listed in Supplemental Table S1.

573 **_Nicotiana benthamiana_ leaf infiltration**

574 *N. benthamiana* leaf infiltration was performed with the Agrobacterium (*Rhizobium*
575 *radiobacter*) strain C58 (GV3101) carrying the respective constructs for confocal microscopy.
576 Agrobacteria cultures were grown overnight at 28°C, centrifuged for 5 min at 4°C at 5000*g*,
577 resuspended in infiltration solution (5 % sucrose, a pinch of glucose, 0.01 % Silwet Gold,
578 150 µM acetosyringone) and incubated for 1 hour at room temperature. Bacterial suspension
579 was set to an OD_{600}=0.4 and infiltrated into the abaxial side of *N. benthamiana* leaves.

580 Expression of pABind and pMDC7 (Curtis and Grossniklaus, 2003; Bleckmann et al., 2010)
581 constructs was induced with a β-estradiol solution (20 µM β-estradiol, 0.1 % Tween 20) 16
582 hours before imaging.

583 **Subcellular localization of fluorescent protein fusions**

584 The creation of TTN5 dominant negative (T30N) and dominant active (Q70L) constructs by
585 introduced point mutations and generation of pro35S::YFP-TTN5 is described in (Mohr et al.,
586 2023). mCherry-tagged constructs were created by overlap-extension PCR. Fluorescent
587 protein was amplified from pABind:mCherry (Bleckmann et al., 2010) using primer pair
588 mCherry B1 and mCh R ns BIND. *TTN5*, $TTN5^{T30N}$ and $TTN5^{Q70L}$ CDS were amplified with a
589 20 bp overlap of mCherry using mCh to TTN5 and TITAN5 stop B2. In a third PCR mCherry-
590 tagged TTN5 constructs were generated with the mCherry B1 and TITAN5 stop B2 primer
591 pair. BP and LR reaction were performed as described above. As destination vector the XVE-
592 driven β-estradiol inducible promoter driven vector pMDC7 (Curtis and Grossniklaus, 2003)
593 was chosen. IRT1-GFP construct, with the GFP at position 173 in the variable, cytoplasmic
594 loop, was cloned by overlap-extension PCR. *GFP* was amplified from pABind:GFP
595 (Bleckmann et al., 2010) using primer pair IG173 F and GI173 R. IRT1 halves were amplified
596 using IRT1 B1 and IG173 R and GI173 R and IRT1 stop B2. In a last PCR IRT1-GFP was
597 amplified with primer pair IRT1 B1 and IRT1 stop B2. BP and LR reaction were performed as
598 described above with pMDC32 (Curtis and Grossniklaus, 2003) as destination vector. Cloning
599 of IRT1-mCherry construct is described in Ivanov et al., (2014) and proIRT1::IRT1-
600 mCitrine/*irt1-1* in Dubeaux et al., (2018). Agrobacteria were transformed with the obtained
601 constructs and tested by *N. benthamiana* leaf infiltration after two days of expression.

602 Localization studies were carried out by laser-scanning confocal microscopy (LSM 780,
603 Zeiss) with a 40x C-Apochromat water immersion objective. YFP constructs were excited at
604 488 nm and detected at 491-560 nm. mCherry or FM4-64 fluorescence was excited at 561 nm
605 and detected at 570-633 nm.

606 **Chemical treatments**

607 Wortmannin (10 µM, Sigma-Aldrich) and plasma membrane dye FM4-64 (165 µM,
608 ThermoFisher Scientific) were infiltrated into *N. benthamiana* leaves. FM4-64 was detected
609 after five min incubation and Wortmannin was incubated for 25 min before checking the
610 treatment effect.

611 **JACoP based colocalization analysis**

612 Colocalization analysis was performed with the ImageJ (Schneider et al., 2012) Plugin Just
613 Another Colocalization Plugin (JACoP) (Bolte and Cordelières, 2006). A comparison of

614 Pearson's and Overlap coefficients was done. Object-based analysis was performed for
615 spotted-structures, adapted by (Ivanov et al., 2014). Percentage of colocalization for both
616 channels was calculated based on distance between geometrical centers of signals. Analysis
617 was conducted in three replicates each (n = 3).

618 **Bimolecular Fluorescence Complementation (BiFC)**

619 The interaction studies of TTN5 and the respective GTPase dominant active ($TTN5^{Q70L}$) or
620 dominant negative ($TTN5^{T30N}$) variants *in planta* were performed by using BiFC. *TTN5*,
621 *$TTN5^{Q70L}$* and *$TTN5^{T30N}$* coding sequences with stop codon were amplified using the primers
622 TITAN5 n-ter B1 and TITAN5 stop B4 (Supplemental Table S1).
623 *IRT1vr* coding sequence with stop codon was amplified using the primers I1L1B3 and I1LB2.
624 Amplifying *EHB1* the primer pair EHB1 n-ter B3 and EHB1 stop B2 was used. *SNX1* coding
625 sequence without stop codon for C-terminal fusion was amplified using the primer SNX1 B3
626 and SNX1 ns B2. Cloning of SNX1 deletion mutants SNX1PX and SNX1BAR was done using
627 the primers SNX1 B3 and PXSNX1 rev and BARSNX1 fwd and SNX1 ns B2 respectively. The
628 used PATL2 constructs are described in (Hornbergs et al., 2022).
629 The amplified PCR products were cloned *via* Gateway BP reaction (Life Technologies) into
630 pDONR221-P1P4 (Invitrogen) or pDONR221-P3P2 (Invitrogen). The obtained constructs were
631 used in an LR reaction (Life Technologies) for cloning into pBiFCt-2in1 vectors (Grefen and
632 Blatt, 2012). Agrobacteria were transformed with correct constructs and used for
633 *N. benthamiana* leaf infiltration. After 48 hours, the mRFP expression control signal and YFP
634 signals were detected by fluorescent microscopy (LSM 780, Zeiss) with a 40x C-Apochromat
635 water immersion objective. YFP constructs were detected at 491-560 nm after exciting at
636 488 nm and mCherry fluorescence was excited at 561 nm and emission detected at 570-
637 633 nm.
638 The BiFC constructs were tested in three independent replicates with three infiltrated leaves
639 each. The vectors pBiFC-2in1-NN and pBiFC-2in1-CN were kindly provided by Dr. Christopher
640 Grefen, Tübingen, Germany.

641 **Förster-Resonance-Energy Transfer Acceptor Photo Bleaching (FRET-APB)**

642 To verify protein-protein interactions of TTN5 and the corresponding GTPase dominant
643 active ($TTN5^{Q70L}$) and dominant negative ($TTN5^{T30N}$) variants the FRET-APB was used. The
644 coding sequences without stop codon were amplified with the primers TITAN5 B1 and TITAN5
645 ns B2, and cloned into the pDONR207 (Invitrogen, BP reaction, Life Technologies). Cloning of
646 pDONR207:IRT1vr and pDONR207:EHB1 is described in Khan et al. (2019). The obtained
647 constructs were used for LR reactions (Life Technologies) with the pABind-GFP, pABind-
648 mCherry and pABind-FRET for C-terminal tagging (Bleckmann et al., 2010). N-terminal GFP-
649 TTN5 constructs were cloned by overlap extension PCR simultaneously with mCherry-TTN5
650 constructs (check paragraph 'Subcellular localization of fluorescent protein fusions'). In the first
651 step the primer pairs GFP B1 with GFP R ns BIND and GFP to TTN5 with TITAN5 stop B2
652 were used with pABind-FRET (Bleckmann et al., 2010) as template for the fluorescent protein
653 coding sequence. The final construct was obtained with the primer pair GFP B1 with TITAN5
654 stop B2. Constructs were cloned into pDONR207 for further cloning into pMDC7 *via* LR
655 reactions. Agrobacteria were transformed and used for *N. benthamiana* leaf infiltration. FRET-
656 APB was performed using laser-scanning confocal microscopy (LSM 780, Zeiss) with a 40x C-
657 Apochromat water immersion objective. GFP was excited at 488 nm and detected at 491-
658 560 nm and mCherry fluorescence was excited at 561 nm and detected at 570-633 nm. GFP

659 and mCherry channels were recorded for five scans. The mCherry signal was then bleached
660 with 70 iterations of maximum laser intensity in a specific region of interest (ROI) which was
661 set to the nucleus. Both channels were detected for additional 20 post-bleaching scans. FRET-
662 APB measurements were performed with a minimum of 10 repetitions ($n \geq 10$).

663 **Statistical analysis**

664 One-way ANOVA was used for statistical analysis and performed in OriginPro 2019. Fisher
665 LSD was chosen as post-hoc test with $p < 0.05$.

666 **ACCESSION NUMBERS**

667 Sequence data from this article can be found in the TAIR and GenBank data libraries under
668 accession numbers: *FRO2* (TAIR: AT1G01580), *EHB1* (TAIR: AT1G70800), *IRT1* (TAIR:
669 AT4G19690), *PATL2* (TAIR: AT1G22530), *TTN5* (TAIR: AT2G18390), and *SNX1* (TAIR:
670 AT5G06140).

671

672 **Acknowledgements**

673 We thank Gintaute Matthäi and Elke Wieneke for excellent technical assistance. We thank
674 Ksenia Trofimov for microscopic help and advice, and Rubek Merina Basgaran for help with
675 interaction studies. We are thankful for the excellent assistance from Stefanie Weidtkamp-
676 Peters and Sebastian Hänsch, members of the Center for Advanced Imaging (CAi) at the
677 Heinrich Heine University.

678 This work was supported by the Deutsche Forschungsgemeinschaft (DFG, German Research
679 Foundation, SFB 1208 project B05 to P.B.). Funding for instrumentation: Zeiss LSM780: DFG-
680 INST 208/551-1 FUGG.

681

682 **Figure Legends**

683

684 **Figure 1. TTN5 interacts with IRT1vr in yeast and in plant cells.**

685 (A), Targeted Y2H assay between BD-IRT1vr (IRT1-variable region) and AD-TTN5. Yeast
686 cotransformations were spotted in 10-fold dilution series ($A_{600} = 10^1$-10^4) on double selective
687 (LW; control) and triple selective +0.5 mM 3-AT (LWH, selection for protein interactions) SD-
688 plates. SNX1/SNX1, positive control (Pourcher et al., 2010), BD-IRT1vr/AD-empty and BD-
689 empty/AD-TTN5 respective negative controls. (B), Schematic representation of the switching
690 mechanism of small GTPases based on TTN5. TTN5 can switch between an inactive GDP-
691 loaded form to an active GTP-loaded one. Intrinsic GDP to GTP nucleotide exchange is
692 unusually high for TTN5 and help by a guanidine exchange factor (GEF) may not be needed,
693 but is not excluded, while GTP hydrolysis has to be catalyzed by a GTPase-activating protein
694 (GAP) (Mohr et al., 2023). GTP-loaded TTN5 can interact with effector proteins for signal
695 transition. (C-G), Validation of TTN5-IRT1vr interaction by bifunctional complementation (BiFC)
696 of split YFP. Genes of interest were fused either to the C- or N-terminal half of split-YFP.
697 Potential interaction is indicated by a complemented YFP signal. mRFP serves as a
698 transformation control. (C-E), nYFP-IRT1vr showed YFP complementation in combination with
699 (C) cYFP-TTN5, (D) dominant-negative (cYFP-TTN5^{T30N}) and dominant-active (cYFP-
700 TTN5^{Q70L}) variants. The complementation takes place in nucleus and cytoplasm predominantly.
701 (F-G), The combinations (F) cYFP-TTN5/nYFP-EHB1Δsig and (G) cYFP-EHB1Δsig/nYFP-
702 IRT1vr served as negative controls. Each combination was tested a minimum of three times

703 with comparable results. Scale bar 50 µm. (H-J), Confirmed interaction via FRET-APB.
704 Significant increase of FRET-efficiency between IRT1vr-mCherry and (H) GFP-TTN5, (I)
705 dominant-negative $TTN5^{T30N}$ or (J) dominant-active $TTN5^{Q70L}$ indicate short protein distances.
706 GFP-fusions are donor-only samples and serve as a negative control. GFP-mCherry-tagged
707 constructs show intra-molecular FRET as a respective positive control. Analysis was done in
708 the nucleus. Each combination was tested a minimum of three times (n = 3) with comparable
709 results. One-way ANOVA with Fisher-LSD post-hoc test was performed. Different letters
710 indicate statistical significance ($p < 0.05$, $n \geq 10$).
711

712 **Figure 2. Heterozygous *ttn5-1*$^{+/-}$ seedlings can have an Fe reductase phenotype.**

713 Heterozygous *ttn5-1*$^{+/-}$ and their wild type sibling seedlings were grown on +/- Fe Hoagland
714 plates for ten days (A-B) or in the two-week system (C-G). All plants were individually
715 genotyped as wild type or *ttn5-1*$^{+/-}$. (A), *ttn5-1*$^{+/-}$ seedlings appeared phenotypically as wild type
716 (WT) siblings. Scale bar 1 cm. (B), Quantified root length of (A). Root length increased under
717 Fe deficient conditions (-Fe, light grey boxes) compared to sufficient conditions (+Fe, dark grey
718 boxes), similar in *ttn5-1*$^{+/-}$ and wild type siblings (+Fe: WT n = 19; *ttn5-1* n = 28; -Fe: WT n =
719 16; *ttn5-1* n = 32). (C), Chlorophyll contents, measured by SPAD values, were similar under
720 both Fe conditions (-Fe, light grey boxes; +Fe, dark grey boxes) and comparable between the
721 plants (+Fe: n = 10; -Fe: n = 9). (D-F), Gene expression data by RT-qPCR of *TTN5, FRO2* and
722 *IRT1* in *ttn5-1*$^{+/-}$ roots compared to wild type siblings in Fe-sufficient (+Fe, black bars) or -
723 deficient (-Fe, grey bars) conditions. (D), *TTN5* expression was reduced under Fe deficient
724 conditions in wild type seedlings. Same took place in *ttn5-1*$^{+/-}$ seedlings under Fe deficiency.
725 (E-F) *FRO2* and *IRT1* expression was induced upon Fe deficiency in wild type and *ttn5-1*$^{+/-}$
726 seedlings in comparable amounts. Data was obtained from three biological replicates (n = 3).
727 (G), Ferric reductase activity was measured as color change due to formation of a Fe^{2+}-
728 ferrozine complex, detected at an OD of 562 nm. The increase in iron reductase activity in
729 response to Fe deficiency was higher in wild type than in *ttn5-1*$^{+/-}$ sibling seedlings. The assay
730 was performed with three (wild type) and four (*ttn5-1*$^{+/-}$) biological replicates (WT n = 3; *ttn5-1*$^{+/-}$
731 n = 4). The experiment was repeated in total three times. In two cases, Fe reductase activity
732 was reduced in *ttn5-1*$^{+/-}$ compared with wild type siblings, and once it was not different. One-
733 way ANOVA with Fisher-LSD as post-hoc test was performed. Different letters indicate
734 statistical significance ($p < 0.05$).
735

736 **Figure 3. TTN5 co-localizes with IRT1 at the plasma membrane and in multi-vesicular**
737 **bodies (MVBs).**

738 (A, D, H) mCherry-TTN5 and its (B, E, I) dominant-negative (mCherry-$TTN5^{T30N}$) and (C, F, J)
739 dominant-active (mCherry-$TTN5^{Q70L}$) variants were co-localized with IRT1-GFP in
740 *N. benthamiana* leaf epidermal cells. (A-C), mCherry-TTN5 and mCherry-TTN5 variants were
741 present at the plasma membrane and in distinct spots together with IRT1. (D-F), Internalized
742 IRT1-GFP was present in mCherry-TTN5 and mCherry-TTN5 variant-containing vesicle-like
743 structures. (G), Schematic illustration of the inhibiting function of the fungal metabolite
744 wortmannin on cellular trafficking routes between the vacuole and the *trans*-Golgi network via
745 MVBs, leading to swelling of MVBs. (H-J), Cells were treated with wortmannin. Swollen MVBs

746 are visible with the GFP- and mCherry-channel, respectively. Colocalization is indicated with
747 filled arrowheads. Scale bar 10 µm.
748

749 **Figure 4. TTN5 interacts with IRT1 regulators EHB1, SNX1 and PATL2.**

750 (A-E, G-P) Bimolecular fluorescence complementation (BiFC) of split YFP experiments with
751 TTN5 and known IRT1 regulators EHB1 (Khan et al., 2019), SNX1 (Ivanov et al., 2014) and
752 PATL2 (Hornbergs et al., 2022). mRFP expression serves as a transformation control. (A-E),
753 TTN5 interacts with EHB1 via the sig domain. (B, D, E), TTN5 and EHB1 showed
754 complementation whereas inactive and active variants were not able to complement split-YFP.
755 (A, C), TTN5 was tested together with EHB1sig (only the sig, signature domain) and with EHB1
756 harboring a deletion of the CAR sig domain (sig domain defined in (Rodriguez et al., 2014;
757 Khan et al. 2019), EHB1∆sig). Deletion of the sig domain resulted in loss of complementation.
758 (F), Interaction between TTN5 and TTN5 variants (GFP-tagged, donor) with EHB1 (mCherry-
759 tagged, acceptor) was confirmed by FRET-APB. EHB1-GFP as donor-only sample (negative
760 control), EHB1-GFP-mCherry for intra-molecular FRET (positive control). Each combination
761 was tested a minimum of three times (n = 3) with comparable results. In this assay, TTN5
762 variants interacted with EHB1. (G-K), BiFC showing that TTN5 interacts with SNX1. (G, I),
763 TTN5 and $TTN5^{Q70L}$ showed complemented YFP signal together with SNX1. (H), No YFP
764 fluorescence was detectable for $TTN5^{T30N}$ with SNX1. (J, K), An interaction took place between
765 TTN5 and the (J) PX and (K) the BAR domain of SNX1. (L-P), BiFC showing that TTN5
766 interacted with PATL2. (L), PATL2 showed complemented YFP signal with N-terminally-tagged
767 TTN5. (M-N), $TTN5^{T30N}$ and $TTN5^{Q70L}$ did not complement YFP with PATL2. (O-P), Deletion
768 mutants of PATL2 showed dependency of the N-terminus for complementation with TTN5. (O)
769 YFP signal was visible for PATL2 N-terminus (PATL2ΔC). (P) On the other hand, the C-
770 terminus alone (PATL2ΔN) had no detectable YFP. Every construct was tested a minimum of
771 three times (n ≥ 3) with similar results. Scale bar 50 µm. One-way ANOVA with Fisher-LSD
772 post-hoc test was performed. Different letters indicate statistical significance ($p < 0.05$).
773

774 **Figure 5. Summary model: Action of TTN5 within the IRT1-regulatory network.**

775 A schematic overview of the identified TTN5 interactors within the IRT1-regulatory network (A)
776 at the plasma membrane (PM) or (B) in the endomembrane compartments of the *trans*-Golgi
777 network (TGN) or multivesicular body (MVB). IRT1 undergoes a constant cycling due to
778 endocytosis from the plasma membrane and either degradation via the lytic pathway in the
779 vacuole or recycling back to the plasma membrane. (A), We identified TTN5 interaction with
780 the large cytosolic, variable region of IRT1. TTN5 and IRT1 co-localize at the plasma
781 membrane (circled 1). PATL2 interacts with the large cytosolic, variable region of IRT1 (IRT1vr)
782 via its N-terminus and is involved in α-tocopherol recruitment to the membrane, to prevent lipid
783 peroxidation induced by IRT1-related iron import (Hornbergs et al., 2022). TTN5 also interacts
784 with the N-terminus of PATL2. A potential TTN5-PATL-IRT1 complex formation is suggested
785 (circled 2). EHB1 interacts with the large cytosolic, variable region of IRT1 via its signature (sig)
786 domain and inhibits IRT1 function at the plasma membrane in a Ca^{2+}-dependent manner (Khan
787 et al. 2019). TTN5 also interacts with EHB1 via the sig domain. A potential TTN5-EHB1-IRT1
788 complex formation is suggested (circled 3). A possible four complex of IRT1, TTN5, PATL2 and
789 EHB1 (circled 4). (B), We found that IRT1 co-localized with SNX1 (Ivanov et al., 2014) and

790 TTN5 in the TGN. IRT1 and TTN5 also co-localized in MVBs. The protein symbols are indicated
791 in the figure legend. The question mark indicates that a potential protein complex may form.
792
793 **Supplemental Figure S1: Localization of fluorescently labeled IRT1 and TTN5 in**
794 **Arabidopsis roots.**
795 IRT1-mCitrine expression (A, C, E) of proIRT1::IRT1-mCit/*irt1-1* seedlings previously described
796 in Dubeaux et al. (2018) in comparison with YFP-TTN5 expression of pro35S::YFP-TTN5 (B,
797 D, F) in Arabidopsis roots. (A-B), IRT1-mCitrine was expressed at the plasma membrane of
798 epidermal cells (A) (empty white arrowhead). YFP-TTN5 expression was localized at the
799 plasma membrane of epidermal cells and other cell types (B). Dotted white lines indicate the
800 position of the longitudinal sections shown in C and D. (C-D), Longitudinal sections highlighted
801 IRT1-mCitrine (C) expression only in epidermal cells compared to nearly ubiquitously
802 expression of YFP-TTN5 (D). (E-F), Next to plasma membrane localization IRT1-mCitrine (E)
803 and YFP-TTN5 (F) were present in intracellular spots (filled white arrowheads). Scale bar
804 10 µm.
805
806 **Supplemental Figure S2. IRT1 colocalization analysis at the plasma membrane and in**
807 **intracellular spots.**
808 (A), Plasma membrane dye FM4-64 confirmed IRT1-GFP expression at the plasma membrane.
809 IRT1 is expressed in a spotted structure, indicating regions of higher transporter accumulation.
810 (B-C), IRT1-GFP colocalized with published IRT1-mCherry (Ivanov et al., 2014) at the plasma
811 membrane (PM) (B) and in intracellular spots (C), confirming correct localization of the IRT1-
812 GFP construct. Scale bar 50 µm. (D), Complementation of rosette growth defect of IRT1-GFP.
813 Rosette sizes of *irt1-1* and pro35S::IRT1-GFP/*irt1-1* were measured 14 days after sowing.
814 IRT1-GFP complemented the growth defect of *irt1-1*. (E-G), JACoP-based colocalization
815 analysis (Bolte and Cordelières, 2006) performed with ImageJ (Schneider et al., 2012). (E-F),
816 Comparison of Pearson's and Overlap coefficients for IRT1-GFP with the three mCherry-TTN5
817 variants at the plasma membrane and in vesicle-like structures was done. (G), Object-based
818 analysis was performed for spotted-structures based on distance between geometrical centers
819 of signals. Analyses were conducted in three replicates each (n = 3).
820 One-way ANOVA with Fisher-LSD post-hoc test was performed. Different letters indicate
821 statistical significance ($p < 0.05$).
822
823 **Supplemental Figure S3. TTN5 effect on its interactors on transcriptional level.**
824 (A-C), Gene expression data by RT-qPCR of TTN5 interactors EHB1, SNX1 and PATL2 in *ttn5-*
825 *1*$^{+/-}$ roots compared to wild type. Plants were grown in the two-week system in Fe-sufficient
826 (+Fe, black bars) or -deficient (-Fe, grey bars) conditions. (A), *EHB1* expression was repressed
827 under Fe-deficient conditions in wild type seedlings. Equal expression levels were present in
828 *ttn5-1* seedlings under both Fe supply conditions. (B), *SNX1* expression was not altered
829 between Fe-sufficient or -deficient conditions in wild type and *ttn5-1* seedlings. (C), Next to
830 *SNX1*, *PATL2* expression did not change upon Fe supply in both wild type and *ttn5-1* seedlings.
831 Data was obtained from three biological replicates (n = 3). One-way ANOVA with Fisher-LSD
832 post-hoc test was performed. Different letters indicate statistical significance ($p < 0.05$).
833
834

References

Adarska P, Wong-Dilworth L, Bottanelli F (2021) ARF GTPases and Their Ubiquitous Role in Intracellular Trafficking Beyond the Golgi. Frontiers in cell and developmental biology **9:** 679046-679046

Anders N, Nielsen M, Keicher J, Stierhof YD, Furutani M, Tasaka M, Skriver K, Jürgens G (2008) Membrane association of the Arabidopsis ARF exchange factor GNOM involves interaction of conserved domains. Plant Cell **20:** 142-151

Antoshechkin I, Han M (2002) The *C. elegans* evl-20 Gene Is a Homolog of the Small GTPase ARL2 and Regulates Cytoskeleton Dynamics during Cytokinesis and Morphogenesis. Developmental Cell **2:** 579-591

Arora D, Van Damme D (2021) Motif-based endomembrane trafficking. Plant Physiology **186:** 221-238

Barberon M, Dubeaux G, Kolb C, Isono E, Zelazny E, Vert G (2014) Polarization of IRON-REGULATED TRANSPORTER 1 (IRT1) to the plant-soil interface plays crucial role in metal homeostasis. Proceedings of the National Academy of Sciences **111:** 8293-8298

Barberon M, Zelazny E, Robert S, Conéjéro G, Curie C, Friml J, Vert G (2011) Monoubiquitin-dependent endocytosis of the IRON-REGULATED TRANSPORTER 1 (IRT1) transporter controls iron uptake in plants. Proceedings of the National Academy of Sciences **108:** E450-E458

Benková E, Michniewicz M, Sauer M, Teichmann T, Seifertová D, Jürgens G, Friml J (2003) Local, Efflux-Dependent Auxin Gradients as a Common Module for Plant Organ Formation. Cell **115:** 591-602

Bhamidipati A, Lewis SA, Cowan NJ (2000) ADP ribosylation factor-like protein 2 (Arl2) regulates the interaction of tubulin-folding cofactor D with native tubulin. Journal of Cell Biology **149:** 1087-1096

Bleckmann A, Weidtkamp-Peters S, Seidel CAM, Simon R (2010) Stem cell signaling in Arabidopsis requires CRN to localize CLV2 to the plasma membrane. Plant physiology **152:** 166-176

Bolte S, Cordelières FP (2006) A guided tour into subcellular colocalization analysis in light microscopy. J Microsc **224:** 213-232

Brumbarova T, Ivanov R (2019) The Nutrient Response Transcriptional Regulome of Arabidopsis. iScience **19:** 358-368

Chen W, Zhou H, Xu F, Yu M, Coego A, Rodriguez L, Lu Y, Xie Q, Fu Q, Chen J, Xu G, Wu D, Li X, Li X, Jaillais Y, Rodriguez PL, Zhu S, Yu F (2023) CAR modulates plasma membrane nano-organization and immune signaling downstream of RALF1-FERONIA signaling pathway. New Phytol **237:** 2148-2162

Cointry V, Vert G (2019) The bifunctional transporter-receptor IRT1 at the heart of metal sensing and signalling. New Phytologist **223:** 1173-1178

Cui M, Gupta SK, Bauer P (2023) Review: Role of the plant-specific calcium-binding C2-DOMAIN ABSCISIC ACID-RELATED (CAR) protein family in environmental signaling. . OSF Preprints

Cui Y, Li X, Chen Q, He X, Yang Q, Zhang A, Yu X, Chen H, Liu N, Xie Q, Yang W, Zuo J, Palme K, Li W (2010) BLOS1, a putative BLOC-1 subunit, interacts with SNX1 and modulates root growth in Arabidopsis. Journal of Cell Science **123:** 3727-3733

Cui Y, Shen J, Gao C, Zhuang X, Wang J, Jiang L (2016) Biogenesis of Plant Prevacuolar Multivesicular Bodies. Molecular Plant **9:** 774-786

Curtis MD, Grossniklaus U (2003) A gateway cloning vector set for high-throughput functional analysis of genes in planta. Plant physiology **133:** 462-469

Dubeaux G, Neveu J, Zelazny E, Vert G (2018) Metal Sensing by the IRT1 Transporter-Receptor Orchestrates Its Own Degradation and Plant Metal Nutrition. Molecular Cell **69:** 953-964.e955

886 **Dümmer M, Michalski C, Essen LO, Rath M, Galland P, Forreiter C** (2016) EHB1 and
887 AGD12, two calcium-dependent proteins affect gravitropism antagonistically in
888 *Arabidopsis thaliana*. J Plant Physiol **206:** 114-124
889 **Eide D, Broderius M, Fett J, Guerinot ML** (1996) A novel iron-regulated metal transporter
890 from plants identified by functional expression in yeast. Proceedings of the National
891 Academy of Sciences **93:** 5624-5628
892 **Eide D, Broderius M, Fett J, Guerinot ML** (1996) A novel iron-regulated metal transporter
893 from plants identified by functional expression in yeast. Proceedings of the National
894 Academy of Sciences of the United States of America **93:** 5624-5628
895 **Fansa EK, Wittinghofer A** (2016) Sorting of lipidated cargo by the Arl2/Arl3 system. Small
896 GTPases **7:** 222-230
897 **Fleming JA, Vega LR, Solomon F** (2000) Function of tubulin binding proteins in vivo. Genetics
898 **156:** 69-80
899 **Foot N, Henshall T, Kumar S** (2017) Ubiquitination and the Regulation of Membrane Proteins.
900 Physiological Reviews **97:** 253-281
901 **Francis JW, Turn RE, Newman LE, Schiavon C, Kahn RA** (2016) Higher order signaling:
902 ARL2 as regulator of both mitochondrial fusion and microtubule dynamics allows
903 integration of 2 essential cell functions. Small GTPases **7:** 188-196
904 **Frost A, Unger VM, De Camilli P** (2009) The BAR Domain Superfamily: Membrane-Molding
905 Macromolecules. Cell **137:** 191-196
906 **Fukaya M, Fukushima D, Hara Y, Sakagami H** (2014) EFA6A, a guanine nucleotide exchange
907 factor for Arf6, interacts with sorting nexin-1 and regulates neurite outgrowth. Journal of
908 Neurochemistry **129:** 21-36
909 **Gaither LA, Eide DJ** (2001) Eukaryotic zinc transporters and their regulation. Biometals **14:**
910 251-270
911 **Geldner N, Anders N, Wolters H, Keicher J, Kornberger W, Muller P, Delbarre A, Ueda T,**
912 **Nakano A, Jürgens G** (2003) The Arabidopsis GNOM ARF-GEF mediates endosomal
913 recycling, auxin transport, and auxin-dependent plant growth. Cell **112:** 219-230
914 **Gratz R, Manishankar P, Ivanov R, Köster P, Mohr I, Trofimov K, Steinhorst L, Meiser J,**
915 **Mai HJ, Drerup M, Arendt S, Holtkamp M, Karst U, Kudla J, Bauer P, Brumbarova**
916 **T** (2019) CIPK11-Dependent Phosphorylation Modulates FIT Activity to Promote
917 Arabidopsis Iron Acquisition in Response to Calcium Signaling. Dev Cell **48:** 726-
918 740.e710
919 **Gratz R, von der Mark C, Ivanov R, Brumbarova T** (2021) Fe acquisition at the crossroad of
920 calcium and reactive oxygen species signaling. Curr Opin Plant Biol **63:** 102048
921 **Grefen C, Blatt MR** (2012) A 2in1 cloning system enables ratiometric bimolecular fluorescence
922 complementation (rBiFC). Biotechniques **53:** 311-314
923 **Grossoehme NE, Akilesh S, Guerinot ML, Wilcox DE** (2006) Metal-Binding
924 Thermodynamics of the Histidine-Rich Sequence from the Metal-Transport Protein
925 IRT1 of *Arabidopsis thaliana*. Inorganic Chemistry **45:** 8500-8508
926 **Guerinot ML** (2000) The ZIP family of metal transporters. Biochimica et Biophysica Acta (BBA)
927 - Biomembranes **1465:** 190-198
928 **Heucken N, Ivanov R** (2018) The retromer, sorting nexins and the plant endomembrane
929 protein trafficking. J Cell Sci **131**
930 **Hornbergs J, Montag K, Loschwitz J, Mohr I, Poschmann G, Schnake A, Gratz R,**
931 **Brumbarova T, Eutebach M, Angrand K, Fink-Straube C, Stühler K, Zeier J,**
932 **Hartmann L, Strodel B, Ivanov R, Bauer P** (2022) SEC14-GOLD protein PATELLIN2
933 binds IRON-REGULATED TRANSPORTER1 linking root iron uptake to vitamin E. Plant
934 Physiol
935 **Hu J** (2021) Toward unzipping the ZIP metal transporters: structure, evolution, and implications
936 on drug discovery against cancer. The FEBS Journal **288:** 5805-5825

Ismail SA, Chen YX, Rusinova A, Chandra A, Bierbaum M, Gremer L, Triola G, Waldmann H, Bastiaens PI, Wittinghofer A (2011) Arl2-GTP and Arl3-GTP regulate a GDI-like transport system for farnesylated cargo. Nat Chem Biol **7:** 942-949

Ismail SA, Vetter IR, Sot B, Wittinghofer A (2010) The Structure of an Arf-ArfGAP Complex Reveals a Ca^{2+} Regulatory Mechanism. Cell **141:** 812-821

Ivanov R, Brumbarova T, Blum A, Jantke A-M, Fink-Straube C, Bauer P (2014) SORTING NEXIN1 is required for modulating the trafficking and stability of the Arabidopsis IRON-REGULATED TRANSPORTER1. The Plant cell **26:** 1294-1307

Ivanov R, Vert G (2021) Endocytosis in plants: Peculiarities and roles in the regulated trafficking of plant metal transporters. Biology of the Cell **113:** 1-13

Jaillais Y, Fobis-Loisy I, Miège C, Rollin C, Gaude T (2006) AtSNX1 defines an endosome for auxin-carrier trafficking in Arabidopsis. Nature **443:** 106-109

Kerkeb L, Mukherjee I, Chatterjee I, Lahner B, Salt DE, Connolly EL (2008) Iron-Induced Turnover of the Arabidopsis IRON-REGULATED TRANSPORTER1 Metal Transporter Requires Lysine Residues Plant Physiology **146:** 1964-1973

Khan I, Gratz R, Denezhkin P, Schott-Verdugo SN, Angrand K, Genders L, Basgaran RM, Fink-Straube C, Brumbarova T, Gohlke H, Bauer P, Ivanov R (2019) Calcium-Promoted Interaction between the C2-Domain Protein EHB1 and Metal Transporter IRT1 Inhibits Arabidopsis Iron Acquisition. Plant Physiology **180:** 1564-1581

Kleine-Vehn J, Dhonukshe P, Sauer M, Brewer PB, Wiśniewska J, Paciorek T, Benková E, Friml J (2008) ARF GEF-dependent transcytosis and polar delivery of PIN auxin carriers in Arabidopsis. Curr Biol **18:** 526-531

Knauer T, Dümmer M, Landgraf F, Forreiter C (2011) A negative effector of blue light-induced and gravitropic bending in Arabidopsis. Plant physiology **156:** 439-447

Kolb C, Nagel M-K, Kalinowska K, Hagmann J, Ichikawa M, Anzenberger F, Alkofer A, Sato MH, Braun P, Isono E (2015) FYVE1 is essential for vacuole biogenesis and intracellular trafficking in Arabidopsis. Plant physiology **167:** 1361-1373

Le CTT, Brumbarova T, Ivanov R, Stoof C, Weber E, Mohrbacher J, Fink-Straube C, Bauer P (2015) ZINC FINGER OF ARABIDOPSIS THALIANA12 (ZAT12) Interacts with FER-LIKE IRON DEFICIENCY-INDUCED TRANSCRIPTION FACTOR (FIT) Linking Iron Deficiency and Oxidative Stress Responses Plant Physiology **170:** 540-557

Li W, Feng Y, Hao C, Guo X, Cui Y, He M, He X (2007) The BLOC Interactomes Form a Network in Endosomal Transport. Journal of Genetics and Genomics **34:** 669-682

Martín-Barranco A, Spielmann J, Dubeaux G, Vert G, Zelazny E (2020) Dynamic Control of the High-Affinity Iron Uptake Complex in Root Epidermal Cells1. Plant Physiology **184:** 1236-1250

Matthus E, Wilkins KA, Davies JM (2019) Iron availability modulates the *Arabidopsis thaliana* root calcium signature evoked by exogenous ATP. Plant Signaling & Behavior **14:** 1640563

Mayer U, Herzog U, Berger F, Inzé D, Jürgens G (1999) Mutations in the PILZ group genes disrupt the microtubule cytoskeleton and uncouple cell cycle progression from cell division in Arabidopsis embryo and endosperm. European Journal of Cell Biology **78:** 100-108

McElver J, Patton D, Rumbaugh M, Liu C-m, Yang LJ, Meinke D (2000) The TITAN5 Gene of Arabidopsis Encodes a Protein Related to the ADP Ribosylation Factor Family of GTP Binding Proteins. The Plant Cell **12:** 1379-1392

Memon AR (2004) The role of ADP-ribosylation factor and SAR1 in vesicular trafficking in plants. Biochim Biophys Acta **1664:** 9-30

Mohr I, Mirzaiebadizi A, Sanyal SK, Chuenban P, Ahmadian MR, Ivanov R, Bauer P (2023) Characterization of the small Arabidopsis thaliana GTPase and ADP-ribosylation factor-like 2 protein TITAN 5. BIORXIV/2023/538563

988 **Montag K, Hornbergs J, Ivanov R, Bauer P** (2020) Phylogenetic analysis of plant multi-
989 domain SEC14-like phosphatidylinositol transfer proteins and structure–function
990 properties of PATELLIN2. Plant Molecular Biology **104:** 665-678
991 **Montag K, Ivanov R, Bauer P** (2023) Role of SEC14-like phosphatidylinositol transfer proteins
992 in membrane identity and dynamics. OSF Preprints
993 **Mori R, Toda T** (2013) The dual role of fission yeast Tbc1/cofactor C orchestrates microtubule
994 homeostasis in tubulin folding and acts as a GAP for GTPase Alp41/Arl2. Mol Biol Cell
995 **24:** 1713-1724, s1711-1718
996 **Nielsen E** (2020) The Small GTPase Superfamily in Plants: A Conserved Regulatory Module
997 with Novel Functions. Annual Review of Plant Biology **71:** 247-272
998 **Peter BJ, Kent HM, Mills IG, Vallis Y, Butler PJ, Evans PR, McMahon HT** (2004) BAR
999 domains as sensors of membrane curvature: the amphiphysin BAR structure. Science
1000 **303:** 495-499
1001 **Pourcher M, Santambrogio M, Thazar N, Thierry A-M, Fobis-Loisy I, Miège C, Jaillais Y,**
1002 **Gaude T** (2010) Analyses of sorting nexins reveal distinct retromer-subcomplex
1003 functions in development and protein sorting in *Arabidopsis thaliana*. The Plant cell **22:**
1004 3980-3991
1005 **Radcliffe PA, Vardy L, Toda T** (2000) A conserved small GTP-binding protein Alp41 is
1006 essential for the cofactor-dependent biogenesis of microtubules in fission yeast. FEBS
1007 Letters **468:** 84-88
1008 **Raposo G, Marks MS, Cutler DF** (2007) Lysosome-related organelles: driving post-Golgi
1009 compartments into specialisation. Current Opinion in Cell Biology **19:** 394-401
1010 **Rath M, Dümmer M, Galland P, Forreiter C** (2020) A gravitropic stimulus alters the distribution
1011 of EHB1, a negative effector of root gravitropism in Arabidopsis. Plant Direct **4:** e00215
1012 **Robinson NJ, Procter CM, Connolly EL, Guerinot ML** (1999) A ferric-chelate reductase for
1013 iron uptake from soils. Nature **397:** 694-697
1014 **Rodriguez L, Gonzalez-Guzman M, Diaz M, Rodrigues A, Izquierdo-Garcia AC, Peirats-**
1015 **Llobet M, Fernandez MA, Antoni R, Fernandez D, Marquez JA, Mulet JM, Albert A,**
1016 **Rodriguez PL** (2014) C2-domain abscisic acid-related proteins mediate the interaction
1017 of PYR/PYL/RCAR abscisic acid receptors with the plasma membrane and regulate
1018 abscisic acid sensitivity in Arabidopsis. Plant Cell **26:** 4802-4820
1019 **Schneider CA, Rasband WS, Eliceiri KW** (2012) NIH Image to ImageJ: 25 years of image
1020 analysis. Nature Methods **9:** 671-675
1021 **Sharer JD, Shern JF, Van Valkenburgh H, Wallace DC, Kahn RA** (2002) ARL2 and BART
1022 Enter Mitochondria and Bind the Adenine Nucleotide Transporter. Molecular Biology of
1023 the Cell **13:** 71-83
1024 **Shin L-J, Lo J-C, Chen G-H, Callis J, Fu H, Yeh K-C** (2013) IRT1 degradation factor1, a ring
1025 E3 ubiquitin ligase, regulates the degradation of iron-regulated transporter1 in
1026 Arabidopsis. The Plant cell **25:** 3039-3051
1027 **Steinmann T, Geldner N, Grebe M, Mangold S, Jackson CL, Paris S, Gälweiler L, Palme**
1028 **K, Jürgens G** (1999) Coordinated polar localization of auxin efflux carrier PIN1 by
1029 GNOM ARF GEF. Science **286:** 316-318
1030 **Sztul E, Chen P-W, Casanova JE, Cherfils J, Dacks JB, Lambright DG, Lee F-JS,**
1031 **Randazzo PA, Santy LC, Schürmann A, Wilhelmi I, Yohe ME, Kahn RA** (2019) ARF
1032 GTPases and their GEFs and GAPs: concepts and challenges. Molecular biology of the
1033 cell **30:** 1249-1271
1034 **Takano J, Tanaka M, Toyoda A, Miwa K, Kasai K, Fuji K, Onouchi H, Naito S, Fujiwara T**
1035 (2010) Polar localization and degradation of Arabidopsis boron transporters through
1036 distinct trafficking pathways. Proc Natl Acad Sci U S A **107:** 5220-5225
1037 **Tanaka H, Kitakura S, De Rycke R, De Groodt R, Friml J** (2009) Fluorescence imaging-
1038 based screen identifies ARF GEF component of early endosomal trafficking. Curr Biol
1039 **19:** 391-397

1040 **Tanaka H, Nodzyński T, Kitakura S, Feraru MI, Sasabe M, Ishikawa T, Kleine-Vehn J,**
1041 **Kakimoto T, Friml J** (2014) BEX1/ARF1A1C is Required for BFA-Sensitive Recycling
1042 of PIN Auxin Transporters and Auxin-Mediated Development in Arabidopsis. Plant and
1043 Cell Physiology **55:** 737-749
1044 **Tian Q, Zhang X, Yang A, Wang T, Zhang W-H** (2016) CIPK23 is involved in iron acquisition
1045 of Arabidopsis by affecting ferric chelate reductase activity. Plant Science **246:** 70-79
1046 **Tzafrir I, McElver JA, Liu Cm C-m, Yang LJ, Wu JQ, Martinez A, Patton DA, Meinke DW**
1047 (2002) Diversity of TITAN functions in Arabidopsis seed development. Plant physiology
1048 **128:** 38-51
1049 **Valencia JP, Goodman K, Otegui MS** (2016) Endocytosis and Endosomal Trafficking in
1050 Plants. Annual Review of Plant Biology **67:** 309-335
1051 **Vernoud V, Horton AC, Yang Z, Nielsen E** (2003) Analysis of the small GTPase gene
1052 superfamily of Arabidopsis. Plant Physiol **131:** 1191-1208
1053 **Vert G, Grotz N, Dédaldéchamp F, Gaymard F, Guerinot ML, Briat J-F, Curie C** (2002)
1054 IRT1, an Arabidopsis Transporter Essential for Iron Uptake from the Soil and for Plant
1055 Growth. The Plant Cell **14:** 1223-1233
1056 **von der Mark C, Ivanov R, Eutebach M, Maurino VG, Bauer P, Brumbarova T** (2020)
1057 Reactive oxygen species coordinate the transcriptional responses to iron availability in
1058 Arabidopsis. Journal of Experimental Botany **72:** 2181-2195
1059 **Yoshinari A, Toda Y, Takano J** (2021) GNOM-dependent endocytosis maintains polar
1060 localisation of the borate exporter BOR1 in Arabidopsis. Biology of the Cell **113:** 264-
1061 269
1062 **Zhang C, Tong C, Cao L, Zheng P, Tang X, Wang L, Miao M, Liu Y, Cao S** (2023) Regulatory
1063 module WRKY33-ATL31-IRT1 mediates cadmium tolerance in Arabidopsis. Plant, Cell
1064 & Environment **46:** 1653-1670
1065

Figure 1

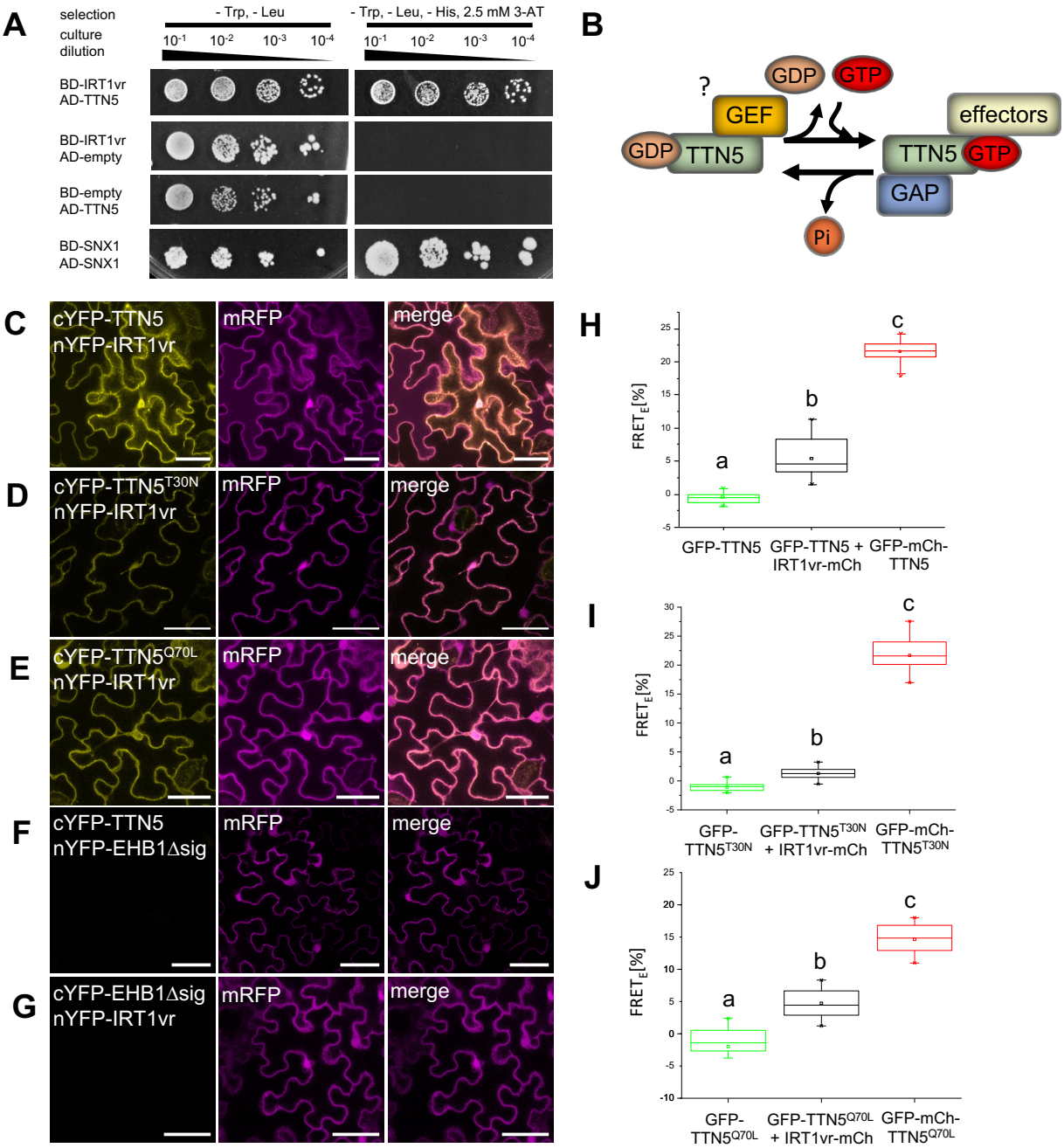
A
selection
culture dilution
- Trp, - Leu
- Trp, - Leu, - His, 2.5 mM 3-AT
10-1 10-2 10-3 10-4
BD-IRT1vr AD-TTN5
BD-IRT1vr AD-empty
BD-empty AD-TTN5
BD-SNX1 AD-SNX1
B
?
GDP
GTP
GEF
effectors
GDP
TTN5
TTN5
GTP
GAP
Pi
C
cYFP-TTN5 nYFP-IRT1vr
mRFP
merge
D
cYFP-TTN5T30N nYFP-IRT1vr
mRFP
merge
E
cYFP-TTN5Q70L nYFP-IRT1vr
mRFP
merge
F
cYFP-TTN5 nYFP-EHB1Δsig
mRFP
merge
G
cYFP-EHB1Δsig nYFP-IRT1vr
mRFP
merge
H
FRETE [%]
a
b
c
GFP-TTN5
GFP-TTN5 + IRT1vr-mCh
GFP-mCh-TTN5
I
FRETE [%]
a
b
c
GFP-TTN5T30N
GFP-TTN5T30N + IRT1vr-mCh
GFP-mCh-TTN5T30N
J
FRETE [%]
a
b
c
GFP-TTN5Q70L
GFP-TTN5Q70L + IRT1vr-mCh
GFP-mCh-TTN5Q70L

Figure 1. TTN5 interacts with IRT1vr in yeast and in plant cells.

(A), Targeted Y2H assay between BD-IRT1vr (IRT1-variable region) and AD-TTN5. Yeast cotransformations were spotted in 10-fold dilution series (A_{600} = 10^1-10^4) on double selective (LW; control) and triple selective +0.5 mM 3-AT (LWH, selection for protein interactions) SD-plates. SNX1/SNX1, positive control (Pourcher et al., 2010), BD-IRT1vr/AD-empty and BD-empty/AD-TTN5 respective negative controls. (B), Schematic representation of the switching mechanism of small GTPases based on TTN5. TTN5 can switch between an inactive GDP-loaded form to an active GTP-loaded one. Intrinsic GDP to GTP nucleotide exchange is unusually high for TTN5 and help by a guanidine exchange factor (GEF) may not be needed, but is not excluded, while GTP hydrolysis has to be catalyzed by a GTPase-activating protein (GAP) (Mohr et al., 2023). GTP-loaded TTN5 can interact with effector proteins for signal transition. (C-G), Validation of TTN5-IRT1vr interaction by bifunctional complementation (BiFC) of split YFP. Genes of interest were fused either to the C- or N-terminal half of split-YFP. Potential interaction is indicated by a complemented YFP signal. mRFP serves as a transformation control. (C-E), nYFP-IRT1vr showed YFP complementation in combination with (C) cYFP-TTN5, (D) dominant-negative (cYFP-TTN5^{T30N}) and dominant-active (cYFP-TTN5^{Q70L}) variants. The complementation takes place in nucleus and cytoplasm predominantly. (F-G), The combinations (F) cYFP-TTN5/nYFP-EHB1Δsig and (G) cYFP-EHB1Δsig/nYFP-IRT1vr served as negative controls. Each combination was tested a minimum of three times with comparable results. Scale bar 50 µm. (H-J), Confirmed interaction via FRET-APB. Significant increase of FRET-efficiency between IRT1vr-mCherry and (H) GFP-TTN5, (I) dominant-negative TTN5^{T30N} or (J) dominant-active TTN5^{Q70L} indicate short protein distances. GFP-fusions are donor-only samples and serve as a negative control. GFP-mCherry-tagged constructs show intra-molecular FRET as a respective positive control. Analysis was done in the nucleus. Each combination was tested a minimum of three times (n = 3) with comparable results. One-way ANOVA with Fisher-LSD post-hoc test was performed. Different letters indicate statistical significance ($p < 0.05$, $n \geq 10$).

Figure 2

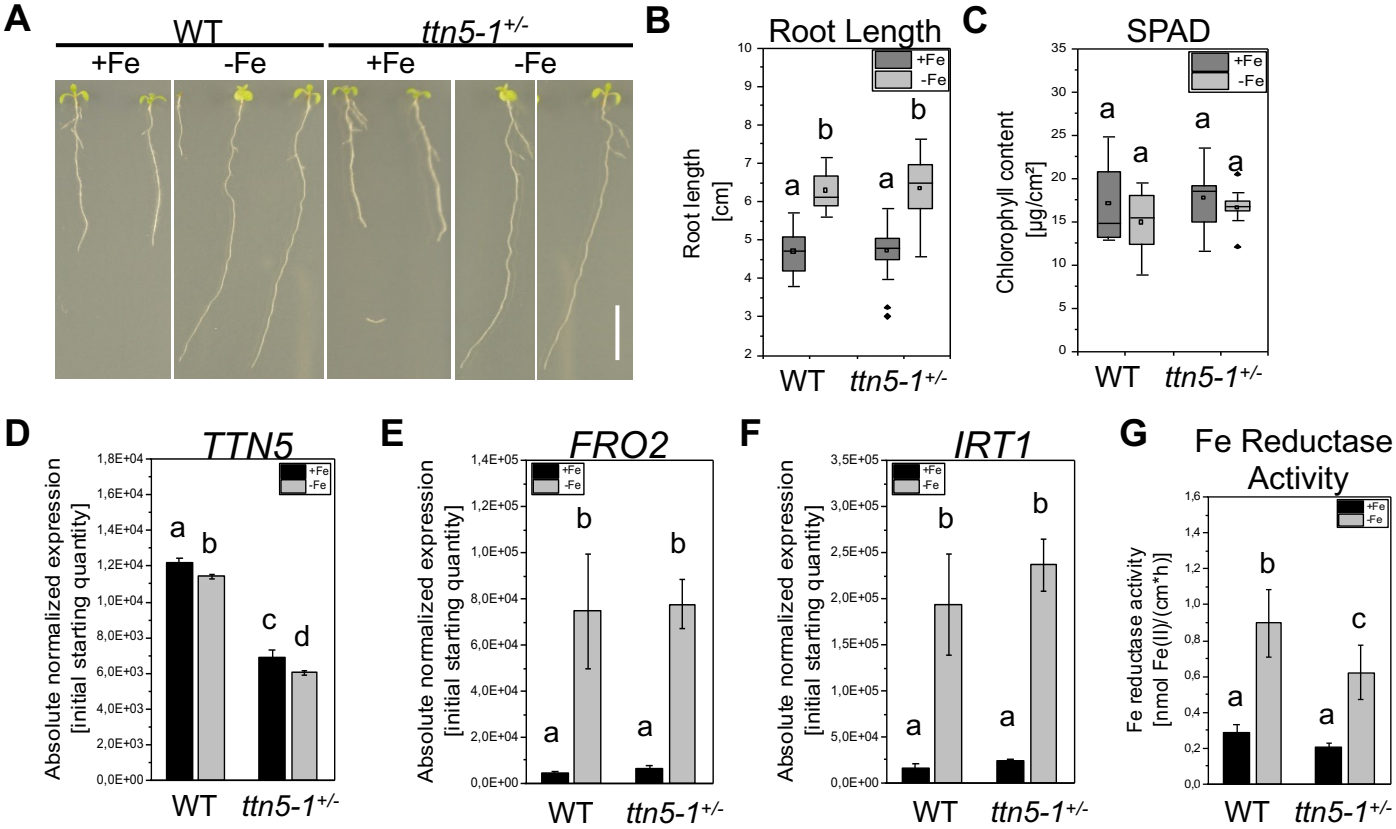
A
WT
ttn5-1+/-
+Fe
-Fe
+Fe
-Fe
B
Root Length
Root length [cm]
+Fe
-Fe
a
b
a
b
WT
ttn5-1+/-
C
SPAD
Chlorophyll content [µg/cm²]
+Fe
-Fe
a
a
a
a
WT
ttn5-1+/-
D
TTN5
Absolute normalized expression [initial starting quantity]
+Fe
-Fe
a
b
c
d
WT
ttn5-1+/-
E
FRO2
Absolute normalized expression [initial starting quantity]
+Fe
-Fe
a
b
a
b
WT
ttn5-1+/-
F
IRT1
Absolute normalized expression [initial starting quantity]
+Fe
-Fe
a
b
a
b
WT
ttn5-1+/-
G
Fe Reductase Activity
Fe reductase activity [nmol Fe(II)/(cm*h)]
+Fe
-Fe
a
b
a
c
WT
ttn5-1+/-

Figure 2. Heterozygous *ttn5-1*$^{+/-}$ seedlings have an Fe reductase phenotype.

Heterozygous *ttn5-1*$^{+/-}$ and their wild type sibling seedlings were grown on +/- Fe Hoagland plates for ten days (A-B) or in the two-week system (C-G). All plants were individually genotyped as wild type or *ttn5-1*$^{+/-}$.

(A), *ttn5-1*$^{+/-}$ seedlings appeared phenotypically as wild type (WT) siblings. Scale bar 1 cm. (B), Quantified root length of (A). Root length increased under Fe deficient conditions (-Fe, light grey boxes) compared to sufficient conditions (+Fe, dark grey boxes), similar in *ttn5-1*$^{+/-}$ and wild type siblings (+Fe: WT n = 19; *ttn5-1* n = 28; -Fe: WT n = 16; *ttn5-1* n = 32). (C), Chlorophyll contents, measured by SPAD values, were similar under both Fe conditions (-Fe, light grey boxes; +Fe, dark grey boxes) and comparable between the plants (+Fe: n = 10; -Fe: n = 9). (D-F), Gene expression data by RT-qPCR of *TTN5, FRO2* and *IRT1* in *ttn5-1*$^{+/-}$ roots compared to wild type siblings in Fe-sufficient (+Fe, black bars) or -deficient (-Fe, grey bars) conditions. (D), *TTN5* expression was reduced under Fe deficient conditions in wild type seedlings. Same took place in *ttn5-1*$^{+/-}$ seedlings under Fe deficiency. (E-F) *FRO2* and *IRT1* expression was induced upon Fe deficiency in wild type and *ttn5-1*$^{+/-}$ seedlings in comparable amounts. Data was obtained from three biological replicates (n = 3). (G), Ferric reductase activity was measured as color change due to formation of a Fe^{2+}-ferrozine complex, detected at an OD of 562 nm. The increase in iron reductase activity in response to Fe deficiency was higher in wild type than in *ttn5-1*$^{+/-}$. The assay was performed with three (wild type) and four (*ttn5-1*$^{+/-}$) biological replicates (WT n = 3; *ttn5-1*$^{+/-}$ n = 4). The experiment was repeated in total three times. In two cases, Fe reductase activity was reduced in *ttn5-1*$^{+/-}$ compared with wild type siblings, and once it was not different.

One-way ANOVA with Fisher-LSD as post-hoc test was performed. Different letters indicate statistical significance ($p < 0.05$).

Figure 3

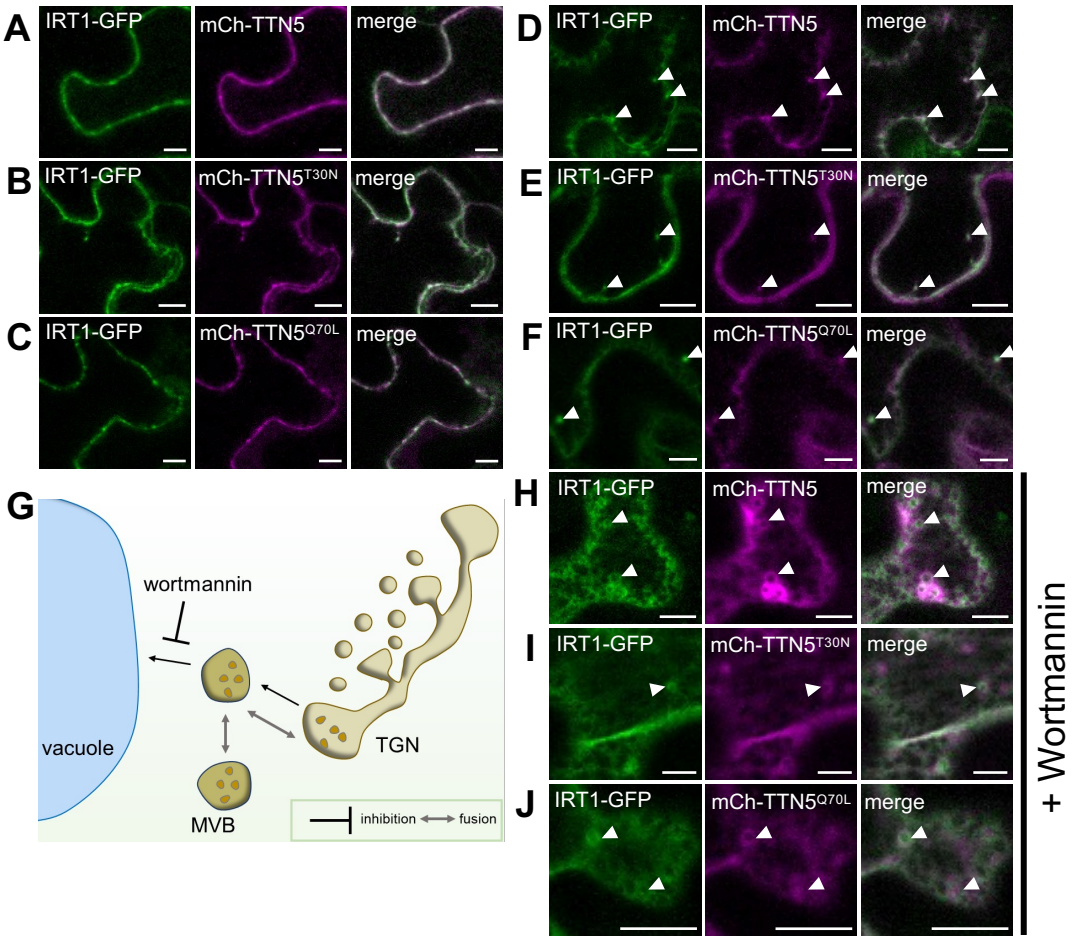
A
IRT1-GFP
mCh-TTN5
merge
B
IRT1-GFP
mCh-TTN5T30N
merge
C
IRT1-GFP
mCh-TTN5Q70L
merge
D
IRT1-GFP
mCh-TTN5
merge
E
IRT1-GFP
mCh-TTN5T30N
merge
F
IRT1-GFP
mCh-TTN5Q70L
merge
G
wortmannin
vacuole
TGN
MVB
inhibition
fusion
H
IRT1-GFP
mCh-TTN5
merge
I
IRT1-GFP
mCh-TTN5T30N
merge
J
IRT1-GFP
mCh-TTN5Q70L
merge
+ Wortmannin

Figure 3. TTN5 co-localizes with IRT1 at the plasma membrane and in multi-vesicular bodies (MVBs).

(A, D, H) mCherry-TTN5 and its (B, E, I) dominant-negative (mCherry-TTN5^{T30N}) and (C, F, J) dominant-active (mCherry-TTN5^{Q70L}) variants were co-localized with IRT1-GFP in *N. benthamiana* leaf epidermal cells. (A-C), mCherry-TTN5 and mCherry-TTN5 variants were present at the plasma membrane and in distinct spots together with IRT1. (D-F), Internalized IRT1-GFP was present in mCherry-TTN5 and mCherry-TTN5 variant-containing vesicle-like structures. (G), Schematic illustration of the inhibiting function of the fungal metabolite wortmannin on cellular trafficking routes between the vacuole and the *trans*-Golgi network via MVBs, leading to swelling of MVBs. (H-J), Cells were treated with wortmannin. Swollen MVBs are visible with the GFP- and mCherry-channel, respectively. Colocalization is indicated with filled arrowheads. Scale bar 10 µm.

Figure 4

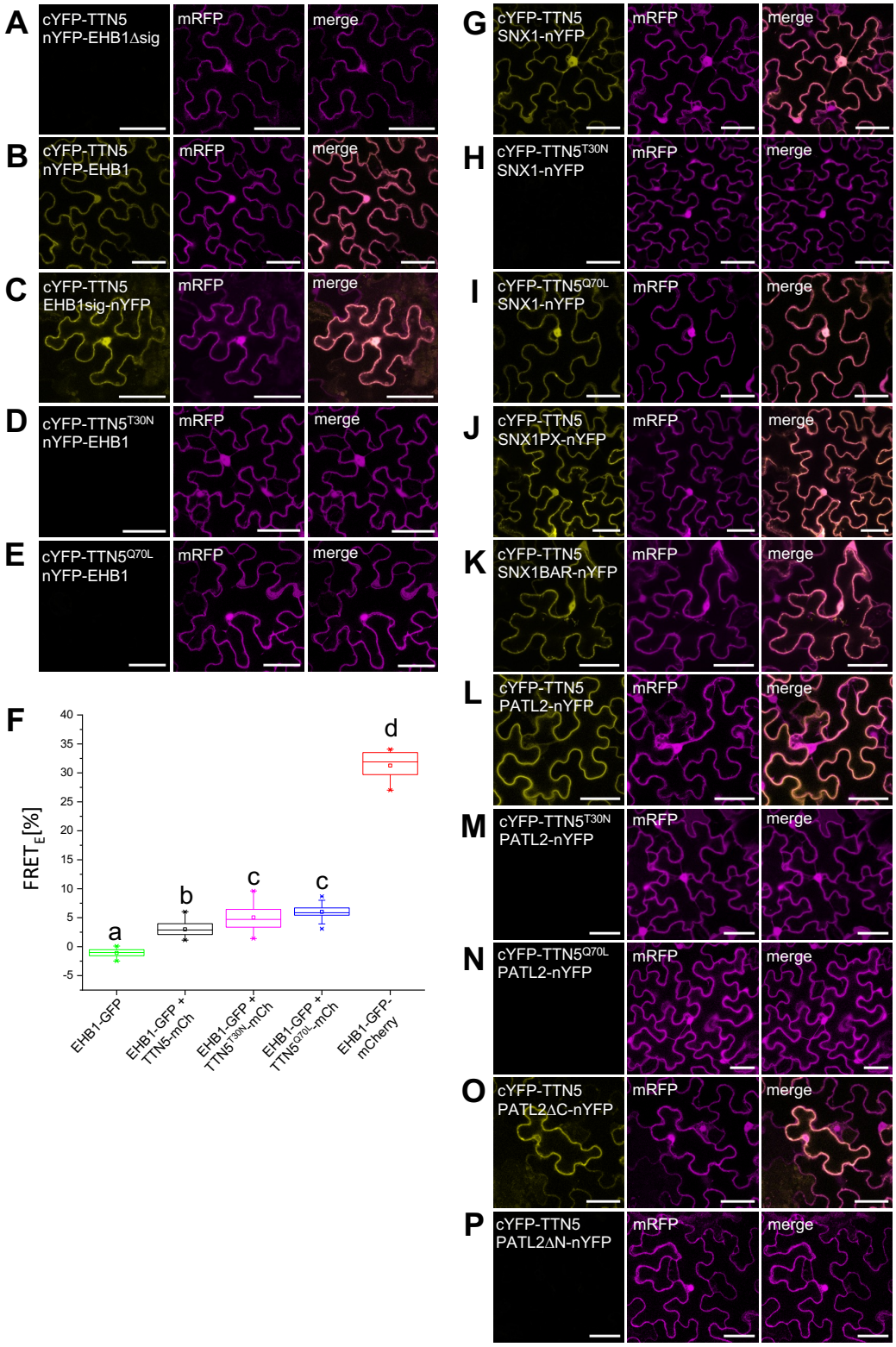
A
cYFP-TTN5
nYFP-EHB1Δsig
mRFP
merge
B
cYFP-TTN5
nYFP-EHB1
mRFP
merge
C
cYFP-TTN5
EHB1sig-nYFP
mRFP
merge
D
cYFP-TTN5T30N
nYFP-EHB1
mRFP
merge
E
cYFP-TTN5Q70L
nYFP-EHB1
mRFP
merge
F
FRETE [%]
40
35
30
25
20
15
10
5
0
-5
a
b
c
c
d
EHB1-GFP
EHB1-GFP + TTN5-mCh
EHB1-GFP + TTN5T30N-mCh
EHB1-GFP + TTN5Q70L-mCh
EHB1-GFP-mCherry
G
cYFP-TTN5
SNX1-nYFP
mRFP
merge
H
cYFP-TTN5T30N
SNX1-nYFP
mRFP
merge
I
cYFP-TTN5Q70L
SNX1-nYFP
mRFP
merge
J
cYFP-TTN5
SNX1PX-nYFP
mRFP
merge
K
cYFP-TTN5
SNX1BAR-nYFP
mRFP
merge
L
cYFP-TTN5
PATL2-nYFP
mRFP
merge
M
cYFP-TTN5T30N
PATL2-nYFP
mRFP
merge
N
cYFP-TTN5Q70L
PATL2-nYFP
mRFP
merge
O
cYFP-TTN5
PATL2ΔC-nYFP
mRFP
merge
P
cYFP-TTN5
PATL2ΔN-nYFP
mRFP
merge

Figure 4. TTN5 interacts with IRT1 regulators EHB1, SNX1 and PATL2.

(A-E, G-P) Bimolecular fluorescence complementation (BiFC) of split YFP experiments with TTN5 and known IRT1 regulators EHB1 (Khan et al., 2019), SNX1 (Ivanov et al., 2014) and PATL2 (Hornbergs et al., 2022). mRFP expression serves as a transformation control. (A-E), TTN5 interacts with EHB1 via the sig domain. (B, D, E), TTN5 and EHB1 showed complementation whereas inactive and active variants were not able to complement split-YFP. (A, C), TTN5 was tested together with EHB1sig (only the sig, signature domain) and with EHB1 harboring a deletion of the CAR sig domain (sig domain defined in (Rodriguez et al., 2014; Khan et al. 2019), EHB1Δsig). Deletion of the sig domain resulted in loss of complementation. (F), Interaction between TTN5 and TTN5 variants (GFP-tagged, donor) with EHB1 (mCherry-tagged, acceptor) was confirmed by FRET-APB. EHB1-GFP as donor-only sample (negative control), EHB1-GFP-mCherry for intra-molecular FRET (positive control). Each combination was tested a minimum of three times (n = 3) with comparable results. In this assay, TTN5 variants interacted with EHB1. (G-K), BiFC showing that TTN5 interacts with SNX1. (G, I), TTN5 and TTN5^{Q70L} showed complemented YFP signal together with SNX1. (H), No YFP fluorescence was detectable for TTN5^{T30N} with SNX1. (J, K), An interaction took place between TTN5 and the (J) PX and (K) the BAR domain of SNX1. (L-P), BiFC showing that TTN5 interacted with PATL2. (L), PATL2 showed complemented YFP signal with N-terminally-tagged TTN5. (M-N), TTN5^{T30N} and TTN5^{Q70L} did not complement YFP with PATL2. (O-P), Deletion mutants of PATL2 showed dependency of the N-terminus for complementation with TTN5. (O) YFP signal was visible for PATL2 N-terminus (PATL2ΔC). (P) On the other hand, the C-terminus alone (PATL2ΔN) had no detectable YFP. Every construct was tested a minimum of three times (n ≥ 3) with similar results. Scale bar 50 µm.

One-way ANOVA with Fisher-LSD post-hoc test was performed. Different letters indicate statistical significance ($p < 0.05$).

Figure 5

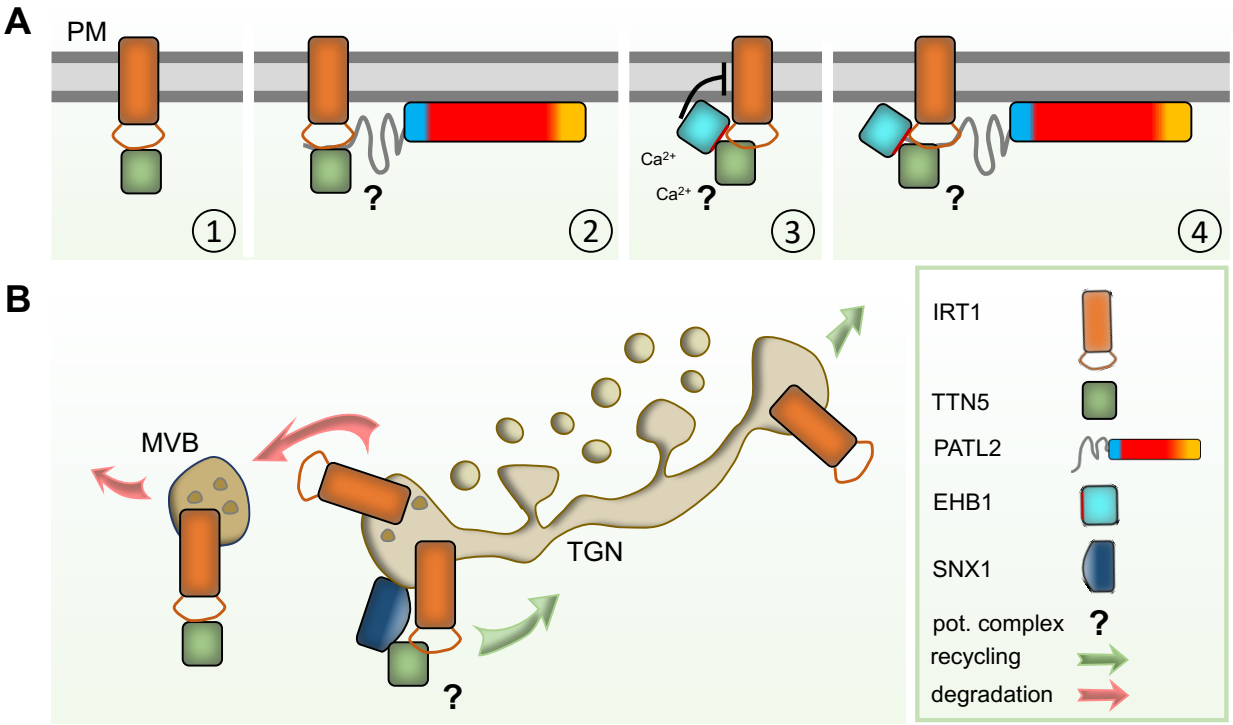
A
PM
1
?
2
Ca2+
Ca2+
?
3
?
4
B
MVB
TGN
?
IRT1
TTN5
PATL2
EHB1
SNX1
pot. complex
?
recycling
degradation

Figure 5. Summary model: Action of TTN5 within the IRT1-regulatory network.

A schematic overview of the identified TTN5 interactors within the IRT1-regulatory network (A) at the plasma membrane (PM) or (B) in the endomembrane compartments of the *trans*-Golgi network (TGN) or multivesicular body (MVB). IRT1 undergoes a constant cycling due to endocytosis from the plasma membrane and either degradation via the lytic pathway in the vacuole or recycling back to the plasma membrane. (A), We identified TTN5 interaction with the large cytosolic, variable region of IRT1. TTN5 and IRT1 co-localize at the plasma membrane (circled 1). PATL2 interacts with the large cytosolic, variable region of IRT1 (IRT1vr) via its N-terminus and is involved in α-tocopherol recruitment to the membrane, to prevent lipid peroxidation induced by IRT1-related iron import (Hornbergs et al. 2022). TTN5 also interacts with the N-terminus of PATL2. A potential TTN5-PATL-IRT1 complex formation is suggested (circled 2). EHB1 interacts with the large cytosolic, variable region of IRT1 via its signature (sig) domain and inhibits IRT1 function at the plasma membrane in a Ca^{2+}-dependent manner (Khan et al. 2019). TTN5 also interacts with EHB1 via the sig domain. A potential TTN5-EHB1-IRT1 complex formation is suggested (circled 3). A possible four complex of IRT1, TTN5, PATL2 and EHB1 (circled 4). (B) We found that IRT1 co-localized with SNX1 (Ivanov et al. 2014) and TTN5 in the TGN. IRT1 and TTN5 also co-localized in MVBs. The protein symbols are explained in the legend. The question mark indicates that the potential protein complex (pot. complex) may form.

Supplemental Figure 1

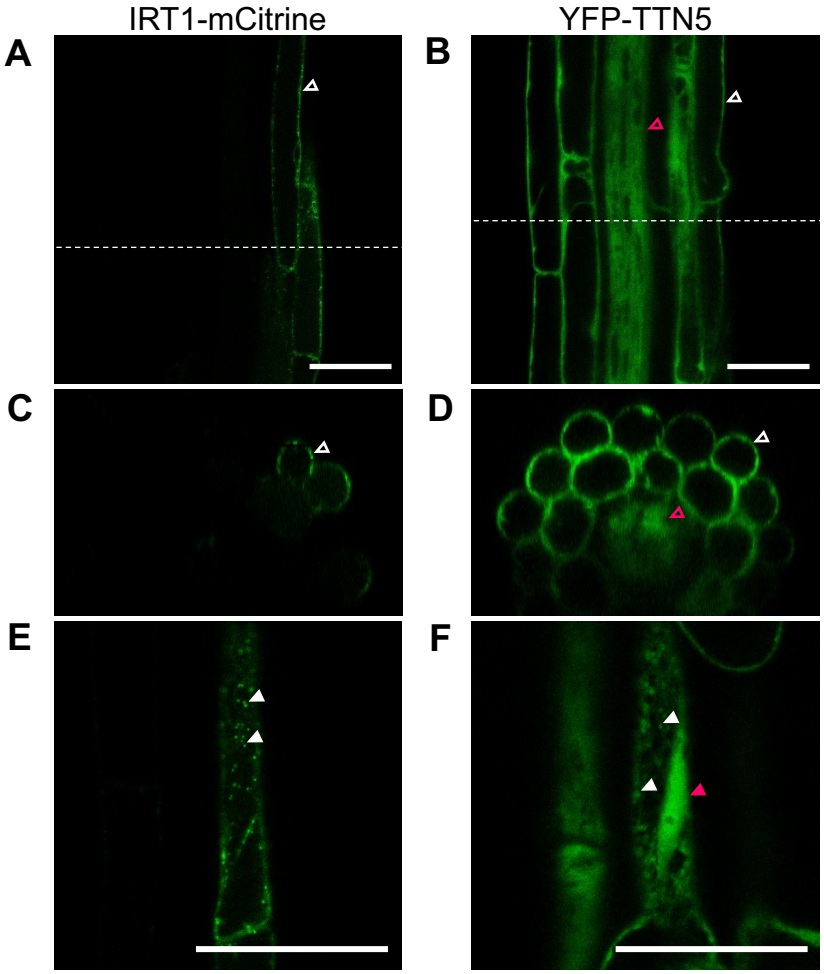

Supplemental Figure S1: Localization of fluorescently labeled IRT1 and TTN5 in Arabidopsis roots.

(A, C, E) IRT1-mCitrine localization in proIRT1::IRT1-mCit/*irt1-1* seedling roots (line previously described in Dubeaux et al. 2018) in comparison with (B, D, F) YFP-TTN5 localization in pro35S::YFP-TTN5/WT seedling roots (line previously described in Mohr et al. 2023). (A, B) Longitudinal sections through the stele. (A), IRT1-mCitrine was present at the plasma membrane of epidermal cells (empty white arrowhead). (B) YFP-TTN5 was localized at the plasma membrane of epidermal cells and other cell types, as well as in the stele (empty magenta arrowhead). Dotted white lines indicate the position of the cross sections shown in C and D. (C-D), Cross sections highlighting (C) IRT1-mCitrine in epidermal cells compared to (D) nearly ubiquitously localized YFP-TTN5. (E-F) Longitudinal section through the epidermis regions. Next to plasma membrane, (E) IRT1-mCitrine and (F) YFP-TTN5 were present in intracellular spots (filled white arrowheads). YFP-TTN5 was also detected in the nucleus (filled magenta arrowhead). Scale bar 10 µm.

Supplemental Figure 2

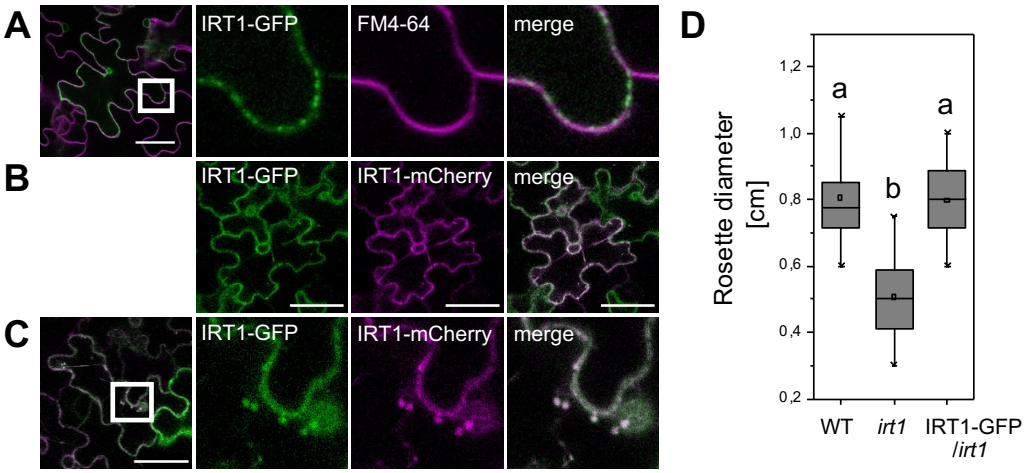

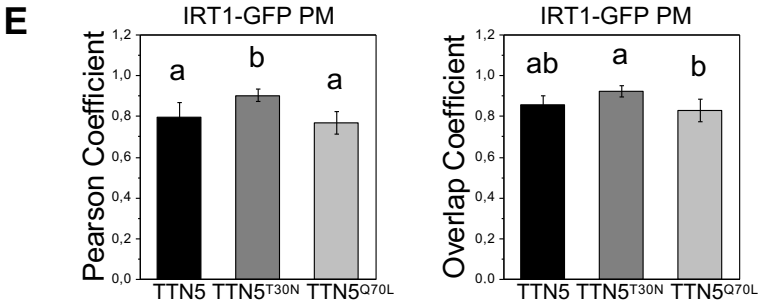

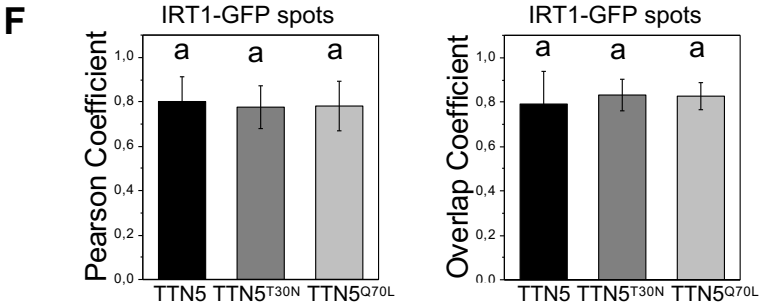

G

Channel		Colocalization spots	
GFP/YFP	mRFP/mCh	GFP/mRFP	mRFP/GFP
IRT1-GFP	mCh-TTN5	64.10±25.58	41.13±28.78
IRT1-GFP	mCh-TTN5^{T30N}	54.44±30.81	36.65±8.25
IRT1-GFP	mCh-TTN5^{Q70L}	82.59±12.71	36.34±9.66

Supplemental Figure S2. IRT1 co-localization analysis at the plasma membrane and in intracellular spots.

(A), Plasma membrane dye FM4-64 indicated IRT1-GFP localization at the plasma membrane. IRT1-GFP is present in a spotted structure, indicating regions of higher transporter accumulation. (B-C), IRT1-GFP co-localized with IRT1-mCherry (Ivanov et al., 2014) (B) at the plasma membrane (PM) and (C) in intracellular spots, confirming correct localization of IRT1-GFP. Scale bar 50 µm. (D), Complementation of rosette growth defect of *irt1-1* by IRT1-GFP. Rosette sizes of *irt1-1* and pro35S::IRT1-GFP/*irt1-1* were measured 14 days after sowing. IRT1-GFP complemented the growth defect of *irt1-1*. (E-G), JACoP-based colocalization analysis of mCherry-TTN5 and variants with IRT1-GFP (Bolte and Cordelières, 2006) performed with ImageJ (Schneider et al., 2012). (E-F), Comparison of (from left to right) Pearson's and Overlap coefficients for IRT1-GFP with mCherry-TTN5, mCherry-TTN5^{T30N} and mCherry-TTN5^{Q70L} (E) at the plasma membrane and (F) in vesicle-like structures. (G), Object-based analysis was performed for spotted-structures based on distance between geometrical centers of signals. Analyses were conducted in three replicates each (n=3). One-way ANOVA with Fisher-LSD post-hoc test was performed. Different letters indicate statistical significance ($p < 0.05$).

Supplemental Figure 3

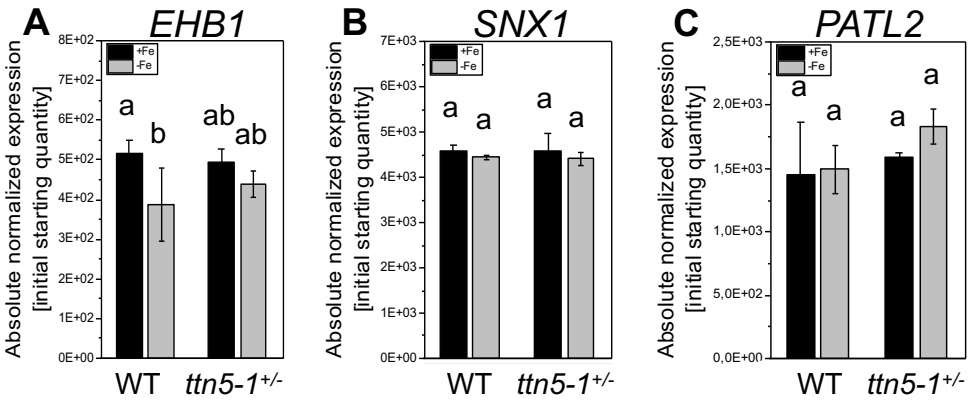

Supplemental Figure S3. Gene expression of *EHB1*, *SNX1* and *PATL2* is not affected in *ttn5-1*$^{+/-}$ plants.

Gene expression data by RT-qPCR of TTN5 interactors *EHB1*, *SNX1* and *PATL2* in *ttn5-1*$^{+/-}$ roots compared to wild type sibling roots. Plants were grown in the two-week system in Fe- sufficient (+Fe, black bars) or -deficient (-Fe, grey bars) conditions. See also Figure 2D-F. (A), *EHB1* expression was down-regulated under Fe deficient conditions in wild type seedlings, while expression levels were not differing in *ttn5-1* seedlings under both Fe supply conditions. (B), *SNX1* expression was not altered between Fe-sufficient or -deficient conditions in wild type and *ttn5-1* seedlings. (C), *PATL2* expression did not change upon Fe supply in both wild-type and *ttn5-1* seedlings. Data were obtained from three biological replicates (n = 3). One-way ANOVA with Fisher-LSD post-hoc test was performed. Different letters indicate statistical significance ($p < 0.05$).